Highlights

Hydrothermal fluorite solubility experiments and mobility of REE in acidic to alkaline solutions from 100 to 250 $^{\circ}\mathrm{C}$ Revision 1

Madison R. Payne, Alexander P. Gysi, Nicole C. Hurtig

- Experimental investigation of fluorite solubility and REE mobility in acidic, mildly acidic and alkaline solutions
- \bullet Reaction textures of fluorite are dissolution-controlled between 100 and 250 $^{\circ}\mathrm{C}$
- Addition of NaCl enhances fluorite dissolution and mobilizes REE in acidic and alkaline fluids
- Mass balance indicates REE-depleted fluorite and REE fluorides precipitation control variations in fluid chemistry
- Fluorite solubility constants are derived between 25 and 250 °C

Hydrothermal fluorite solubility experiments and mobility of REE in acidic to alkaline solutions from 100 to 250 $^{\circ}\mathrm{C}$

Revision 1

Madison R. Payne^{a,b}, Alexander P. Gysi^{a,b,*}, Nicole C. Hurtig^a

^aDepartment of Earth and Environmental Sciences, New Mexico Institute of Mining and Technology, Socorro, 87801, NM, USA

^bNew Mexico Bureau of Geology and Mineral Resources, New Mexico Institute of Mining and Technology, Socorro, 87801, NM, USA

Abstract

Fluorite is a common vein mineral in critical mineral deposits that are overprinted by hydrothermal processes. Its chemistry potentially reflects the mobilization conditions of rare earth elements (REE) in these hydrothermal fluids. However, the controls of temperature and fluid chemistry (i.e. pH and salinity) on fluorite solubility and coupled REE mobilization is still uncertain. In this study, batch-type experiments were conducted to investigate REE mobility in aqueous fluids controlled by the solubility of fluorite at temperatures between 100 and 250 °C. Natural fluorite crystals from Cooke's Peak (New Mexico) were equilibrated with aqueous solutions of variable starting pH (2–10), salinities (0 and 15 wt.% NaCl), and initial REE concentrations (0 and 0.5 ppm). Reacted fluorite crystals display dissolution-controlled reaction textures (i.e., etch pits and dissolution channels along fluorite cleavage

Email address: Alexander.Gysi@nmt.edu (Alexander P. Gysi)

^{*}Corresponding author

planes), which are most pronounced in experiments conducted in acidic fluids and at elevated temperature. Addition of NaCl enhances considerably fluorite dissolution, in both acidic and alkaline solutions, which is also reflected by the compositions of the reacted solutions displaying an increase in Ca, F, and REE concentrations. The overall fluorite solubility is controlled by the association behavior of HF⁰ at acidic conditions, and by the formation of Ca chloride, Ca hydroxyl, and Na fluoride complexes, which become enhanced by addition of NaCl, including in mildly acidic and alkaline solutions. Mass balance calculations were used to compare the REE stoichiometry of unreacted fluorite crystals with measured REE concentrations in the reacted solutions, which reveal several possible controls on REE mobility: i) stoichiometric release of REE upon fluorite dissolution; ii) precipitation of secondary REE-depleted fluorite; and/or iii) precipitation of secondary light REE fluorides, which were observed to form on fluorite crystals surfaces in the REE-doped experiments. Fluorite solubility constants (K_{sp}) were regressed with available low temperature solubility data using the equation $\log K_{\rm sp} =$ A+BT+C/T+Dlog(T) (T, temperature in K) valid between 25–250 °C. Fitted coefficients yield: A= 171.180, B= 0.01477, C= -7794.10, D= -64.6634. The experimental results have important implications for geochemical modeling of natural systems, where fluorine controls the mobility of REE, and can be enhanced by addition of NaCl in both acidic and alkaline solutions. Therefore, the salinity of magmatic-hydrothermal fluids plays a crucial role in mobilizing REE during the formation of hydrothermal fluorite veins. Keywords: fluorite, rare earth elements, mineral deposits, solubility products, hydrothermal experiments

1. Introduction

25

The rare earth elements (REE) are considered critical minerals that are used for building components in the high-tech and green technology industries, such as for instance, permanent magnets in wind turbines and electronic components in computers and cellphones (Hatch, 2012; Goodenough et al., 2018). Carbonatites and (per)alkaline igneous complexes are host to the largest REE mineral deposits, and while their emplacement is largely magmatic, hydrothermal aqueous fluids commonly play a significant role in the mobilization of REE in their final evolution stages (Gysi and Williams-Jones, 2013; Gysi et al., 2016; Elliott et al., 2018; Walter et al., 2021). Prominent examples include the giant Bayan Obo carbonatite deposit in China (Smith and Henderson, 2000; Smith et al., 2000, 2015) and the world class Strange Lake peralkaline granitic REE-Zr-Nb deposit in Canada (Salvi and Williams-Jones, 1990; Gysi and Williams-Jones, 2013; Gysi et al., 2016; Vasyukova and Williams-Jones, 2018, 2019). To date, most of the fluid-rock interaction models of hydrothermal REE 16 transport have focused on the role of aqueous speciation and REE-ligand complexes (Kolonin and Shironosova, 2002; Gysi and Williams-Jones, 2013; Migdisov and Williams-Jones, 2014; Migdisov et al., 2016; Perry and Gysi, 2018). Another factor that influences the mobility of REE includes the solubility of REE-bearing minerals, such as the REE fluorides, fluorocarbonates, and phosphates, some of which have only recently been determined experimentally (Gysi and Williams-Jones, 2015; Voigt et al., 2016; Gysi et al., 2018; Gysi and Harlov, 2021).

Fluorite veins are commonly observed in association with critical min-

eral deposits and other magmatic-hydrothermal systems, and their chemical signatures are useful indicators of fluid-rock interaction (Möller et al., 1998; Gagnon et al., 2003; Schwinn and Markl, 2005; Schönenberger et al., 2008; Nadoll et al., 2018). However, we do not yet have a solid understanding of the factors controlling the REE signatures in fluorite and the effect of dissolved fluorine on REE mobility in carbonatite and peralkaline systems. The substitution of REE into the fluorite crystal structure is generally thought to be correlated with the difference in ionic radii between REE³⁺ and Ca²⁺; the light (L)REE (e.g. La³⁺ with 1.16 Å) are preferentially incorporated into fluorite over the heavy (H)REE (e.g. Lu³⁺ with 0.98 Å) when comparing their ionic radii with Ca^{2+} (1.12 Å) in 8-fold coordination (Shannon, 1976). Hydrothermal REE-doped fluorite synthesis experiments by Van Hinsberg et al. (2010) have shown that at 60 °C the REE partitioning behavior can be explained by the lattice strain model (Blundy and Wood, 2003, 1994), and is less influenced by the presence of different ligands (i.e., $\mathrm{Cl}^-,\,\mathrm{NO}^-_3$ and $\mathrm{SO_4^{2-}}).$ In contrast, recent REE-doped calcite synthesis experiments at 200 °C (Perry and Gysi, 2020) have shown that pH and fluid chemistry can affect the REE fluid-mineral partitioning behavior and substitution mechanisms in hydrothermal minerals. The same was observed by Curti et al. (2005) for the precipitation of Eu³⁺ in calcite at ambient temperature. To our knowledge, hydrothermal fluorite solubility experiments are sparse >100 °C (e.g. Strübel, 1965; Richardson and Holland, 1979; Kurovskaya and Malinin, 1983; Tropper and Manning, 2007; Zhang et al., 2017), and none of these studies have investigated the mobility of REE.

50

Here, we investigate the effects of temperature, pH and fluid compositions

(NaCl and REE concentration) on the solubility of fluorite and the consequent release of REE in hydrothermal fluids, and present a series of fluorite dissolution experiments conducted in batch reactors between 100 and 250 °C. The experimental data are evaluated using the GEMS code package (Kulik et al., 2013; Miron et al., 2015) and the MINES thermodynamic database (Gysi, 2017) for determining aqueous speciation, saturation of secondary REE minerals, and retrieving fluorite solubility products. This approach provides new insight into how fluid chemistry and fluorite solubility both affect REE mobility in hydrothermal aqueous fluids.

60 2. Methods

2.1. Starting materials

Natural fluorite crystals were collected from the Surprise mine in the Cooke's Peak Pb-Zn-Cu-Au sulfide carbonate replacement and fluorite historic mining district in New Mexico (North and Tuff, 1986; Simmons, 2019). Three generations of transparent fluorite zones were identified, including a green, purple, and blue fluorite with distinct REE signatures (Fig. 1 and Table 1). The green fluorite displays the highest chondrite-normalized LREE values (>10–100) and is occasionally intergrown with minor purple fluorite which shows an overall REE depletion. The blue fluorite displays a LREE depletion and HREE enrichment in comparison to the green fluorite. The green fluorite was selected for the experiments due to its inclusion-free transparent crystals and relatively high REE concentrations (Table 1). Fluorite crystals were hand-picked for the experiments, cleaved into millimeter-sized fragments and ultrasonically cleaned in a 0.5% HCl solution for 15 minutes.

The fluorite crystals were then transferred into MilliQ water (18 M Ω ·cm), ultrasonically cleaned for 20 minutes, and dried in an oven.

Acidic stock solutions of pH 2 and 4 were prepared by titrating trace metal 77 grade HCl (Inorganic Ventures, $0.1001 \pm 0.0005 \text{ M}$) into MilliQ water to adjust the pH values. Alkaline stock solutions of pH 10 were prepared using trace metal grade NaOH (Inorganic Ventures, $0.1002 \pm 0.0005 \,\mathrm{M}$) and titrated into MilliQ water. The pH values in the stock solutions were measured at room temperature using a Thermo Scientific Orion Star A111 benchtop pH meter and a 9157BNMD Orion Triode combined pH-temperature electrode. The electrode was calibrated using Fisher Scientific commercial buffer solutions (pH of 2, 4, 7, 10; accuracy of ± 0.01). Saline stock solutions of 15 wt.% NaCl (Alfa Aesar, 99.998% metals basis) were prepared by dissolving 15 grams NaCl in 100 grams of previously prepared pH 2, 4, and 10 stock solutions. The REE-doped stock solutions were prepared using a REE custom standard (SCP Science, 10 ppm; NIST traceable certified standard), which was first diluted in MilliQ water to a concentration of 0.5 ppm total REE followed by a titration of NaOH/HCl to reach the desired starting pH values of 2 and 4, respectively. The alkaline stock solution of pH 10 was not doped with REE due to precipitation of REE at room temperature. The compositions of the starting experimental solutions are listed in Table 2.

2.2. Experimental method

Hydrothermal fluorite solubility experiments were carried out for up to 14 days in 45 mL Teflon-lined stainless steel batch-type reactors (Parr Instruments Company[®], 4744) between 100 and 250 °C at saturated water vapor pressure. A series of kinetic experiments were sequentially quenched between

1 and 14 days to determine approach to steady state Ca and F concentra-101 tions. These kinetic runs were tested in the experiments with a starting 102 pH of 2 at 150 °C, pH of 4 at 150 °C, and pH of 10 at 250 °C. Duplicate 103 experiments were also conducted and quenched at various time periods to 104 determine experimental uncertainty.

Each reactor was first loaded with 25 g of the starting experimental solu-105 tion and a single mm-sized fluorite crystal. The experimental starting condi-106 tions (Table 2) were subdivided based on starting pH at room temperature 107 (i.e., acidic, mildly acidic, and alkaline), addition of NaCl, and/or doping 108 with REE. Masses of both the starting solution and fluorite crystal were de-109 termined prior to loading the reactor and after quenching the experiments. 110 The sealed reactors were loaded into a furnace (ColeParmer[®], EW-33858-111 70) and the temperature was maintained within 2 °C of the experimental set point and monitored via an Omega® temperature logger and K-type thermo-113 couple, located at the center of the furnace. At the end of an experiment, the reactors were removed from the furnace and quenched in a cold water bath in less than 20 minutes to minimize reaction upon cooling. The reacted fluorite crystals were then removed and rinsed with MilliQ water. The quenched solutions were then pipetted into separate vials including a 5 mL sample for F analysis and a 20 mL acidified sample (2% HNO₃, Fisher Scientific, trace metal grade) for REE, Ca, and Na analysis. The Teflon liners were then rinsed with MilliQ water, followed by a 24-hour soak in a concentrated nitric acid solution, a MilliQ water soak, and dried in an oven before starting a new experiment.

2.3. Analytical methods

Prior to analysis, the unreacted and reacted fluorite crystals were mounted 125 in epoxy and polished, followed by carbon coating for analysis using scanning electron microscopy (SEM). Crystal zoning, reaction textures, and sec-127 ondary mineral precipitates were studied using a TESCAN MIRA3 LMH 128 Schottky field-emission SEM at the Mineral and Materials Characterization 120 Facility at the Department of Geology and Geological Engineering, Colorado School of Mines. An accelerating voltage of 15 keV and a working distance of ~ 10 mm were used for analysis. Backscattered electron (BSE) imaging was performed using a TESCAN motorized retractable annular, single-crystal yttrium aluminum garnet (YAG) detector. Semi-quantitative energy disper-134 sive (EDS) analyses were conducted using a Bruker XFlash 6/30 silicon drift X-ray spectrometer. Additional BSE imaging was conducted on a Cameca 4-spectrometer SX-100 electron microprobe at the New Mexico Bureau of Geology and Mineral Resources, New Mexico Institute of Mining and Technology. 139

The REE compositions of the unreacted and reacted fluorite samples from
the Cooke's Peak mining district in New Mexico were measured using laser
ablation inductively coupled plasma mass spectrometry (LA-ICP-MS) at the
United States Geological Survey (USGS) federal center in Denver, Colorado.
The following isotopes were quantified: ²³Na, ²⁴Mg, ²⁹Si, ³¹P, ⁸⁸Sr, ⁸⁹Y, ¹³⁹La,
¹⁴⁰Ce, ¹⁴¹Pr, ¹⁴⁶Nd, ¹⁴⁷Sm, ¹⁵³Eu, ¹⁵⁷Gd, ¹⁵⁹Tb, ¹⁶³Dy, ¹⁶⁵Ho, ¹⁶⁶Er, ¹⁶⁹Tm,
¹⁷²Yb, ¹⁷⁵Lu. The LA system consists of a Photon Machines Analyte G2 (193
nm, 4 ns excimer) with a HelEX ablation cell. Ablation was carried out using
a 30 µm square spot size for a duration of 30 seconds, a laser energy density

of $\sim 10.5 \text{ J/cm}^2$, and a repetition rate of 5 Hz. Two cleaning ablation shots were applied before collecting background and sample signal. The ablated samples were then carried to an Agilent 8900 ICP-MS via a He carrier gas mixed with argon. Dwell times were set to: 5 ms for Na, Si, P; 10 ms for Mg, Ca, and Sr; 20 ms for Y, La, Ce, Pr, Nd, Sm, Eu, Gd, Tb, Dy, Ho, Er, 153 Tm, Yb, Lu. Concentrations, drift, spikes, and detection limit calculations 154 were conducted using the protocol of Longerich et al. (1996) and the SILLS 155 software program developed by Guillong et al. (2008). Signals were calibrated using the NIST 612 glass as an external standard, and ⁴⁴CaO was used as 157 the internal standard assuming ideal fluorite stoichiometry. Yttrium counts 158 were used to correct for drift. Additional standards measured include the 159 USGS synthetic basaltic glass reference materials (BCR-2g and BHVO-g) to 160 compare measured with standard values for method development. 161

Dissolved Ca and Na concentrations in the quenched experimental solu-162 tions were measured in acidified (2% HNO₃ matrix) samples using an Agilent 163 7900 ICP optical emission spectrometry (OES) instrument at the Analytical 164 Chemistry Laboratory in the New Mexico Bureau of Geology and Mineral Resources, New Mexico Institute of Mining and Technology. Analytical standards were prepared from single Ca (Inorganic Ventures, CGCA1, 1001 ± 3 ppm) and Na (Inorganic Ventures, CGNA1, 1002 ±4 ppm) standards and 168 diluted with a 2% HNO₃ (Fisher Scientific, trace metal grade) blank matrix 169 solution. Based on repeated standard analysis, the analytical precision for both Ca and Na were better than 3% in the concentration range of the experimental solutions. The analytical precision (95% confidence level) based on repeated standard analysis was better than 1% for Ca at concentrations

between 2×10^{-6} and 5×10^{-4} mol/kg (0.1–20 ppm), and 2% for Na at concentrations between 2×10^{-5} and 2×10^{-3} mol/kg (0.5–50 ppm).

Dissolved REE concentrations were measured in acidified (2% HNO₃ ma-176 trix) samples using an Agilent 7500 quadruple ICP-MS at the Analytical Chemistry Laboratory in the New Mexico Bureau of Geology and Mineral 178 Resources, New Mexico Institute of Mining and Technology. An in-line he-179 lium gas collision cell was used to reduce REE oxide formation. A series of di-180 luted multi-REE standards (Inorganic Ventures, CMS-1, 10 ± 0.04 ppm) were prepared for external calibration. Individual La, Ce, Nd, and Eu standards 182 (Inorganic Ventures, 1000 ± 5 ppm) were prepared, and if necessary, used to 183 correct for REE oxide formation using the same method as described by Gysi 184 et al. (2018) and Aries et al. (2000). Samples were spiked in-line with indium 185 (SCP Science, NIST traceable) as an internal standard for drift corrections. The analytical precision (95% confidence level) based on repeated standard 187 analysis is 10% at concentrations between 1×10^{-10} and 1×10^{-9} mol/kg (0.01– 188 0.1 ppb), better than 3% at concentrations above 1×10^{-9} mol/kg (>0.1 ppb). 180 The detection limits were determined using repeated analysis of the proce-190 dural blank (5σ) and range between 1 and 5 ppt.

Dissolved F concentrations were measured with a Dionex ion chromatograph (ICS-5000 DP-5) with an IonPac® AS22 analytical column, AG22
guard column, ASRS® 300 anion self-regenerating suppressor, and Thermo
Scientific conductivity detector. The standard current used for the selfregenerating suppressor was 9 mA. The in-line eluent used was 4.5 mM
sodium carbonate and 1.4 mM sodium bicarbonate (Dionex AS22 Eluent
Concentrate). The injection volume was 50 µL. A series of dilute multi-

analyte (Inorganic Ventures, IC-FAS-1A, 19.98 ± 0.08 ppm F) IC standards were prepared for calibration. The analytical precision (95% confidence level) based on repeated standard analysis is 2.3% for F concentrations between 1×10^{-6} and 1×10^{-5} mol/kg (0.02–0.2 ppm), and 1.4% for concentrations above 1×10^{-5} to 1×10^{-4} mol/kg (>0.2–2 ppm).

204 2.4. Data treatment

Aqueous speciation, mineral saturation indices, and pH were calculated 205 at the experimental pressures and temperatures using the GEMS code pack-206 age (Kulik et al., 2013) and GEMSFITS (Miron et al., 2015) from the mea-207 sured cation and anion concentrations in the reacted experimental solutions. 208 Thermodynamic properties of aqueous species, gases and minerals in the Ca-Na-REE-F-Cl-O-H component system were taken from the MINES ther-210 modynamic database (https://geoinfo.nmt.edu/mines-tdb/). Aqueous REE 211 species of interest include the REE fluoride and chloride complexes deter-212 mined experimentally by Migdisov et al. (2009) and the REE hydroxyl com-213 plexes from Haas et al. (1995). The latter were theoretically extrapolated to high temperatures, and need revision, but are currently the only available internally consistent dataset for all of the REE hydroxyl species (Migdisov 216 et al., 2016). The thermodynamic properties of other aqueous species were 217 taken from the SUPCRT92 program and slop98.dat database (Helgeson et al., 218 1981; Tanger and Helgeson, 1988; Johnson et al., 1992; Shock et al., 1997; Sverjensky et al., 1997), which were implemented in the GEMS code package and referred as Supert92 hereafter. This dataset was recently updated for Na-, Ca-, and Cl-bearing aqueous species using the GEMSFITS optimization program (Miron et al., 2015) and based on more recent experimental data

(Miron et al., 2016, 2017), which are included in the MINES database. The thermodynamic properties of fluorite were taken from Robie and Hemingway 225 (1995) and data for solid REEF₃ and REE(OH)₃ from Diakonov et al. (1998) and Navrotsky et al. (2015). Activity models and equations of state are implemented in GEMS using the TSolMod library (Wagner et al., 2012). Activity coefficients for charged 229 species were calculated using the extended Debye-Hückel equation (Robinson 230 and Stokes, 1968) and corresponding background electrolyte models for NaCl, 231 NaOH, and HCl (Helgeson et al., 1981; Wagner et al., 2012). The activity of neutral species was calculated from the osmotic coefficient. The thermo-233 dynamic properties of aqueous species were calculated at elevated temperature according to the revised Helgeson-Kirkham-Flowers (HKF) equation of 235 state (Helgeson et al., 1981; Shock and Helgeson, 1988; Tanger and Helgeson, 1988; Shock et al., 1992). The equation of state used for gases was the Peng-Robinson-Stryjek-Vera with critical parameters from Frenkel et al. (1994), Proust and Vera (1989), and Stryjek and Vera (1986).

3. Results

41 3.1. Fluorite dissolution textures and secondary REE minerals

Representative BSE images of the fluorite crystals indicate alteration textures dominantly controlled by dissolution features and varying in intensity as a function of temperature, pH, and salinity of the experiments (Figs. 2–4). The effects of reacting the fluorite crystals with acidic and alkaline experimental solutions are compared in Figure 2. Dissolution textures are more prominent in the experiments conducted at acidic conditions, which are characterized by irregular leached crystal surfaces, triangular etch pits, and etch pit trails along fluorite cleavage planes (Fig. 2c-d). Dissolution textures in alkaline solutions are characterized by the development of pitting along the fluorite crystal cleavage planes near the crystal edges but only reaching about 50 to 100 μ m into the fluorite (Fig. 2 e-f).

Temperature considerably increases the intensity of fluorite dissolution 253 textures, which is particularly pronounced by comparison of the 100 °C (Fig. 254 2) experiments versus the experiments conducted at 150 and 250 °C (Fig. 255 3). The dissolution textures are characterized by the development of etch pit networks and irregular dissolution channels along fluorite cleavage planes, 257 which can reach hundreds of micrometers into the fluorite crystals. Differ-258 ences in dissolution textures observed in acidic and alkaline solutions appear 259 to be more pronounced in experiments conducted at 150 and 250 °C. Fluorite crystals reacted in the acidic solutions develop strongly leached and irregular 261 rounded surfaces (Fig. 3a-b), whereas crystals reacted in the alkaline solu-262 tions preserve straight crystal edges and elongate pit trails reaching about 20 to 50 μ m into the fluorite crystals (Fig. 3c-d). 264

Addition of NaCl significantly increases the intensity of fluorite dissolution textures with the formation of pervasively rounded crystal surfaces
in both acidic and alkaline pH solutions (Fig. 4). In these experiments,
triangular etch pits are absent. Fluorite reacted in saline mildly acidic solutions displays similar textures but the rounded crystal rims preserve some of
the small-scale dissolution textures (i.e., etch pits and dissolution channels;
Supplementary Materials, Appendix B). Fluorite reacted in saline alkaline
experimental solutions display the development of interconnected dissolu-

tion channels reaching $\sim 100\text{-}200~\mu\mathrm{m}$ into the altered fluorite crystal surfaces (Fig. 4d).

Minor secondary fluorite can be observed on the reacted fluorite surfaces 275 with representative SEM images shown in Figure 5. This fluorite displays an anhedral habit and preferentially forms small (1-5 μ m) crystals in etch 277 pits, and was observed in experiments conducted in mildly alkaline and alka-278 line solutions. Secondary REE minerals were only identified in experiments 279 initially doped with 0.5 ppm REE (Fig. 5). Backscattered electron images 280 show bright REE minerals typically precipitated along the cleavage planes of the reacted fluorite. The secondary REE minerals were analyzed using SEM-282 EDS and are composed of La, Ce, Pr, Nd, Y, and F, with a stoichiometry 283 corresponding to REE fluoride (REEF₃), i.e. fluocerite (Fig. 5). 284

Fluorite crystal fragments reacted with acidic to mildly acidic REE-doped experimental solutions display only minimal deviations from the REE concentrations of the unreacted green fluorite (Fig. 1; Supplementary Materials, Tables A1 and A2). The REE composition was therefore not significantly modified upon reaction of the fluorite crystals with the hydrothermal solutions. This also corroborates with the subtle zoning observed in BSE images of some fluorite crystal fragments that preserved their original compositions (Fig. 2).

293 3.2. Fluid chemistry

294 3.2.1. Kinetic experiments and fluorite solubility

Major element compositions of the quenched experimental solutions are listed in Table 3 and the results for each set of kinetic experiments are shown in Figure 6. The total dissolved Ca and F concentrations indicate an ap-

proach to steady state after 1–2 days of reaction. A significantly higher fluorite solubility is observed in the experiments with an acidic pH, with about 1 to 2 orders of magnitude higher concentrations in dissolved Ca and F in comparison to the mildly acidic and alkaline pH solutions. Addition of ~15 wt.% NaCl increases fluorite solubility, particularly in the mildly acidic to alkaline solutions (Fig. 6).

The ionic activities of aCa²⁺ and aF⁻ were calculated at the experimental temperatures using measured Ca and F concentrations and the GEMS code package (full speciation listed in the Supplementary Materials, Table A4) to derive the reaction quotient (Q_{sp} , i.e. solubility products) for the fluorite dissolution reaction,

$$CaF_2 = Ca^{2+} + 2F^-$$
 (1)

$$Q_{\rm sp} = a \operatorname{Ca}^{2+} \times (a \operatorname{F}^{-})^{2} \tag{2}$$

The reaction quotients were then compared to calculated equilibrium constants (K_{sp}) of the fluorite dissolution reaction in order to calculate the fluorite saturation index (SI),

$$SI = log(Q_{sp}/K_{sp})$$
 (3)

Calculated values for aqueous ion activities, Q_{sp} , and SI (Table 3 and Supplementary Materials, Table A3), and their variations as a function of temperature are shown in Figure 7. A plot of $\log Q_{sp}$ vs. temperature between
100 and 250 °C (Fig. 7a) indicates a systematic retrograde solubility trend
in the NaCl-free solutions. The highest $\log Q_{sp}$ values are found in the experiments with mildly acidic and alkaline solutions, both plotting close to
the calculated fluorite saturation and suggesting approach to equilibrium in

these experiments. Variation of the solubility product at each temperature generally reflects the kinetic experiments and the experimental uncertainty based on duplicate runs; values cluster close together for experiments carried out for 2 days or longer. Departure from the calculated fluorite saturation is significant for experiments conducted in saline solutions and some of the acidic solutions as well as experiments conducted at 100 °C (Fig. 7a). Experiments in saline solutions display about an order of magnitude lower Q_{sp} values than in other experiments.

Departure from fluorite saturation can also be further investigated by 319 inspecting the calculated fluorite saturation indices (Fig. 7b), which gen-320 erally corroborate with the pH of the starting experimental solutions. The 321 alkaline solutions are close to saturation with fluorite with an average SI 322 between 150 and 250 °C of -0.15 ± 0.17 ; the mildly acidic experiments display slightly lower average SI values of -0.43 ± 0.21 ; and the experiments in acidic solutions were more undersaturated with average SI values of -0.96 ± 0.14 . Experiments with ~ 15 wt.% NaCl have lower calculated SI values of -1.17 ± 0.46 . The calculated SI in the REE-doped experiments have values of -3.44 ±1.54 (Supplementary Materials, Table A3) and indicate a strong undersaturation with fluorite possibly due to precipitation of secondary REE fluorides. 330

Kinetic experiments and calculated fluorite saturation indices indicate that experiments in mildly acidic and alkaline solutions provide the most reliable data to evaluate the solubility constants of fluorite as a function of temperature between 150 and 250 °C. The systematic shift in calculated $\log Q_{sp}$ and SI values for the saline experiments and some of the acidic HCl-

bearing solutions, indicate a possible need to revise data for the Ca chloride species (i.e., $CaCl^+$ and $CaCl_2(aq)$) and NaF^0 involved in the speciation calculations, which can result in the lower calculated activities for Ca^{2+} (Table 3). The latter influence the calculated reaction quotients and saturation indices of fluorite (Eq. 2).

$3.2.2. REE \ solubility$

360

Measured REE concentrations in the quenched experimental solutions 342 are summarized in Table 4. Kinetic runs indicate a rapid approach to steady state with REE concentrations leveling off after 1–2 days of reaction (Fig. 8), and minimal perturbation by precipitation of secondary REE fluorides (if present). These trends also indicate rapid equilibration between fluorite and the reacted solutions, corroborating the chemistry of Ca and F (Fig. 6) Figure 9 shows a comparison of the REE concentrations measured in 348 the experimental solutions as a function of temperature, salinity and pH. The REE concentrations are chondrite-normalized to eliminate the effects 350 of crustal abundance (i.e., odd/even atomic numbers for each of the REE), 351 allowing to make a comparison to REE profiles in the unreacted fluorite (Fig. 352 1). These plots indicate that pH and salinity play a major role in controlling 353 the solubility of REE. In the absence of NaCl, the highest REE concentrations are found in the quenched fluids from experiments conducted in 355 acidic solutions with chondrite-normalized values ranging between $\sim 1 \times 10^{-3}$ and 1×10^{-1} . Experiments conducted in mildly acidic and alkaline solutions had overall lower chondrite-normalized values ranging between $\sim 1 \times 10^{-5}$ and 1×10^{-3} .

Temperature has a minimal influence on the solubility of REE between

100 and 250 °C. Some of the variations shown in Figure 9 are related to reaction time as shown by a higher chondrite-normalized REE profiles. In the acidic solutions, some variations in LREE can be related to the initial fluorite crystals used the experiments (i.e., blue fluorite is depleted in LREE over the green fluorite); these can easily be distinguished by the small variations in REE profiles within one group of fluorite crystals. The overall LREE and HREE variations in the mildly acidic and alkaline solutions are very similar and display an overall flat REE profile in comparison to the experiments conducted in acidic solutions (Fig. 9b-c).

For all investigated pH, addition of NaCl results in a significant increase in REE concentrations by several orders of magnitude (Table 4). This increase is more pronounced in alkaline solutions, where the chondrite-normalized values increase from $\sim 1 \times 10^{-3}$ to $\sim 1 \times 10^{0}$ approaching values observed in the acidic solutions.

375 4. Discussion

4.1. Controls on fluorite solubility and derivation of solubility constants

Comparison of fluid chemistry (Fig. 6–7; Table 3) with fluorite reaction textures (Figs. 2–4) indicates that salinity and pH exert a stronger control on fluorite solubility than temperature between 100 and 250 °C. In turn, fluorite solubility has a primary control on the release of REE and availability of F for the formation of secondary REE fluorides and/or fluorite enriched/depleted in REE. The experiments indicate that the overall mobility of REE is fluorite dissolution-controlled. This contrasts to coupled dissolution-precipitation mechanisms (Putnis and Putnis, 2022) which have

been reported for the metasomatism of apatite and monazite in high temperature-pressure experiments (300–900 °C and 100–1000 MPa) and deduced
from REE mineral textures in natural systems (Harlov et al., 2005, 2011;
Betkowski et al., 2016; Harlov et al., 2016; Patel et al., 2022). This would
be reflected, for example, by the replacement of apatite by secondary apatite
plus xenotime and monazite, while preserving the overall crystal morphology
(i.e., pseudomorphic replacement).

The control of fluid chemistry on fluorite solubility in our experiments can be described by the following sets of aqueous complex formation reactions:

$$H^{+} + F^{-} = HF^{0} \tag{4}$$

$$Ca^{2+} + Cl^{-} = CaCl^{+}$$

$$\tag{5}$$

$$Ca^{2+} + 2Cl^{-} = CaCl_{2}^{0}$$
 (6)

$$Ca^{2+} + OH^{-} = Ca(OH)^{+}$$
 (7)

$$Na^+ + F^- = NaF^0 \tag{8}$$

Driving these reactions to the right will lower the Ca²⁺ and F⁻ activities in the fluid and drive fluorite solubility (Eq. 1). In acidic and mildly acidic solutions, fluorite solubility is controlled by Reactions 4–6 (see also Supplementary Materials Tables, calculated species activities), which explains why addition of HCl and NaCl enhances fluorite solubility. In alkaline solutions, the formation of Ca hydroxyl species becomes important with increased pH (Reaction 7). The formation of NaF⁰ becomes important in the experiments with NaCl (Supplementary Materials, Table A4). A similar observation was made in the study by Richardson and Holland (1979), in which the solubility of fluorite was measured at >100 °C in solutions containing variable amounts of NaCl, CaCl₂ and other salts.

Fluorite solubility products derived from our experimental data (Eqs: 1–30 are compared with available literature data between 25–350 °C in Figure 10. Based on the fluorite saturation indices presented earlier (Fig. 7), experiments conducted at 100 °C and experiments with NaCl were excluded for the derivation of the solubility constant $(K_{\rm sp})$ of fluorite because their low SI indicate that they may not have reached equilibrium.

The high temperature experiments by Richardson and Holland (1979) 411 (except their data at 100 °C), Strübel (1965), and fitted data by Nordstrom 412 and Jenne (1977), diverge considerably from our measured fluorite solubil-413 ity products (Fig. 10). These literature data also display large discrepancies with the predicted solubility products calculated from a combination of aqueous species (Ca²⁺ and F⁻) from Sucprt92 (slop98.dat) recently optimized by Miron et al. (2017), with the properties of fluorite from Robie and Hemingway (1995). These discrepancies can result from several factors. Firstly, fluorine was analyzed using ion selective electrodes, which is less accurate (i.e., formation of potentials) and has higher detection limits than IC used in our study. Secondly, the experiments by Richardson and Holland (1979) were carried out in gold capsules using a weight loss technique with only a 422 few mg solutions recovered in comparison to this study, where Ca was measured reliably using ICP-OES and about 25 g solution recovered. Finally, the calculated activities of Ca²⁺ and F⁻ species need to be carefully evaluated at elevated temperature. Species that may need to be re-evaluated include some of the fluoride species (NaF⁰, CaF⁺, and HF⁰) that strongly affect the calculated F⁻ activities and fluorite solubility in saline and acidic solutions and hence can result in apparent strongly undersaturated solutions (Fig. 7).

The fluorite solubility products from Garand and Mucci (2004) and Henry (2018) at 25 °C closely approach each other, whereas the solubility constants derived by Zhang et al. (2017) are slightly higher (Fig. 10). Therefore, our experimental solubility products were only combined with the values from Garand and Mucci (2004) at 25 °C, Henry (2018) at 25–50 °C, Richardson and Holland (1979) at 100 °C, then fitted to the following equation to derive the solubility constants as a function of temperature:

$$logK_{sp} = A + BT + C/T + Dlog(T)$$
(9)

The fitted coefficients, solubility constants, and thermodynamic properties are listed in Table 5. The fitted curve is shown in Figure 10. The solubility constant retrieved at 25 °C and 1 bar has a $\log K_{\rm sp}$ value of -10.56, which is in excellent agreement with the recent fluorite solubility analysis by Nordstrom (2022) with a $\log K_{\rm sp}$ value of -10.57 \pm 0.08. Further, the standard thermodynamic properties of reaction can be retrieved from the solubility constants and the fitted coefficients (Table 5):

$$logK_{sp} = \frac{-\Delta_r G^{\circ}}{Rln(10)T} \tag{10}$$

$$\Delta_r G^{\circ} = \Delta_r H^{\circ} - T \Delta_r S^{\circ} \tag{11}$$

$$\Delta_r H^{\circ} = (R \ln(10)(BT^2 - C + DT/\ln(10)))/1000 \tag{12}$$

where $\Delta_r G^{\circ}$, $\Delta_r H^{\circ}$, and $\Delta_r S^{\circ}$ are the standard Gibbs energy, enthalpy and entropy of reaction (in Eq. 2); T is the temperature in Kelvin; R is the ideal gas constant. At reference temperature (298.15 K) and pressure (1 bar) the retrieved values yield: $\Delta_r G^{\circ}_{298.15K} = 60.29 \text{ kJ mol}^{-1}$ and $\Delta_r H^{\circ}_{298.15K}$ = 14.05 kJ mol⁻¹. Combining these values with the properties of aqueous species (Table 5) yields the fluorite standard properties of formation from the elements at 298.15 K and 1 bar of: $\Delta_f G^{\circ}_{fluorite}$ of -1176.6 kJ mol⁻¹ and $\Delta_f H^{\circ}_{fluorite}$ of -1227.9 kJ mol⁻¹. For comparison, the thermodynamic properties for fluorite from Robie and Hemingway (1995) are listed with a $\Delta_f G^{\circ}_{fluorite}$ value of -1175.3 kJ mol⁻¹ and a $\Delta_f H^{\circ}_{fluorite}$ value of -1228.0 kJ mol⁻¹. Also, the standard entropy derived from the solubility data (Eq. 11) yields 72.3 J mol⁻¹K⁻¹, which is quite close to the value of 68.9 J mol⁻¹K⁻¹ from Robie and Hemingway (1995). This gives confidence in the fitted experimental data between 25–254 °C as presented in Table 5.

Including the solubility products from Zhang et al. (2017) or the higher temperature data (200–260 °C) by Richardson and Holland (1979) yields inconsistent regressed thermodynamic properties of reaction. Trying to add these values to the data regression yielded standard enthalpy of formation values diverging by 10–20 kJ/mol and entropy values diverging by 30-40 J mol⁻¹K⁻¹ in comparison to the values by Robie and Hemingway (1995). We therefore do not recommend combining these solubility data with our experimental data to derive fluorite solubility constants at elevated temperature.

9 4.2. Controls of secondary fluorite and REE minerals on REE mobility

The following two simplified reactions explain how the formation of secondary minerals further affects REE mobility and stoichiometry of the experimental solutions:

$$(Ca_x, REE_y)F_2(s) = xCa^{2+} + yREE^{3+} + 2F^-$$
 (13)

$$REE^{3+} + 3F^{-} = REEF_3(s) \tag{14}$$

Reaction 13 represents the dissolution of fluorite and stoichiometric re-463 lease of REE when driven to the right, or precipitation of secondary fluorite 464 with a priori unknown REE concentrations when driven to the left. Reac-465 tion 14 represents the solubility of REE fluorides. Minor precipitation of 466 fluorite was observed on some of the reacted crystal surfaces, and secondary REE fluorides were identified using SEM-EDS but only in the REE-doped experiments (Fig. 5). Due to the small sizes and small abundance of sec-469 ondary fluorite, it is difficult to evaluate whether Reaction 13 or 14 control the mobility of REE upon release of REE and F during fluorite dissolution. Comparison of chondrite-normalized LREE variations in the quenched experimental solutions (Fig. 9) with the REE profiles measured in the unreacted fluorite crystals (Fig. 1), indicates a possible control by formation 474 of secondary minerals. This is particularly pronounced for La, Ce, Pr, and 475 Nd, that are depleted over heavier REE in many of the experiments (Fig. 9). Two approaches are presented here to further evaluate the controls of secondary mineral formation on REE mobility including the calculation of mineral saturation indices and a mass balance approach. 479

The first approach consists of evaluating the potential for secondary REE mineral formation by calculating the saturation indices (SI) of REE fluorides and hydroxides. The SI were determined from calculated ion activities (Supplementary Materials, Tables A3 and A4), which were derived from the compositions of the quenched experimental solutions and the speciation calculations using the GEMS code package (Kulik et al., 2013). Calculated SI indicate that the experimental solutions are generally closer to saturation

with REE fluorides than with the REE hydroxides; the latter are mostly undersaturated except in a few of the alkaline and NaCl-bearing solutions 488 (Supplementary Materials, Table A3). Experiments in acidic and mildly 489 acidic solutions as well as experiments in NaCl-solutions are close to saturation with REE fluorides. This behavior corroborates with the higher fluorite 491 solubility, and hence higher F⁻ activity in these solutions in comparison to 492 experiments conducted in alkaline solutions. The LREE fluorides (i.e., LaF₃, 493 CeF₃, SmF₃, and EuF₃) show typically the highest affinity for saturation in 494 the experimental solutions, whereas the HREE fluorides are all undersaturated. Experiments in the REE doped solutions are also close to saturation 496 with the LREE fluorides and some of the HREE fluorides, particularly in the 497 high temperature experiments conducted at 250 °C (Supplementary Materials, Appendix B3).

The second approach consists of mass balance calculations to evaluate the stoichiometry of REE upon fluorite dissolution and potential for precipitation of secondary REE-bearing fluorite versus REE fluorides. Comparison of the measured Ca, F, and REE concentration ratios in the quenched experimental solutions (Tables 3–4) with measured LA-ICP-MS data of the unreacted fluorite (Table 1) allows determining the following logarithmic ratios:

$$log \frac{(REE/Ca)_{fluid}}{(REE/Ca)_{solid}} \tag{15}$$

$$log \frac{(REE/F)_{fluid}}{(REE/F)_{solid}} \tag{16}$$

where $(REE/Ca)_{fluid}$ and $(REE/F)_{fluid}$ are the molality ratios of REE, Ca and F measured in the quenched experimental solutions; $(REE/Ca)_{solid}$ and $(REE/F)_{solid}$ are the ratios expected from the stoichiometric dissolution of fluorite. For Equations 15 and 16, a value equal to 0 indicates a stoichiometric REE release upon fluorite dissolution. A value greater than 0
indicates that the REE remain in solution and an affinity for the formation
of secondary REE-depleted fluorite (i.e., lowering Ca and F concentrations).
Conversely, a value less than 0 indicates precipitation of secondary REE minerals and sequestration of REE from solution due to either the formation of
REE fluorides or REE-enriched fluorite. Distinction between the latter two
can be made by comparing the REE/Ca and REE/F ratios as depicted in
Figure 11.

In acidic solutions, the REE/Ca and REE/F ratios plot close to the sto-512 ichiometric dissolution line for fluorite (Figs. 11a,d). The LREE deviate 513 from that trend, most notably La and Ce that plot above the stoichiometric 514 line. In contrast, the HREE plot all close to the stoichiometric line, except Y. We interpret these trends to indicate the formation of LREE depleted and slightly Y enriched fluorite, with an overall lack of LREE fluoride precipitation. These trends contrast with the predicted saturation indices for La- and Ce-fluorides that seem to overpredict the affinity for LREE fluoride precipitation in those experiments (Supplementary Materials, Appendix B3). Nevertheless, these observations are in line with some of the chondritenormalized REE profiles depicted in Figure 9a. Lanthanum is enriched in the acidic solutions over other REE, whereas Y is present in similar concentrations than Ho and Dy. Because Y presents a positive anomaly in the unreacted fluorite, the fluid chemistry indicates that some Y must have precipitated into secondary fluorite to reach similar concentrations to Ho and Dy in the reacted solutions.

In mildly acidic and alkaline solutions (Figs. 11b-c and 11e-f), there is 528 a notable switch in REE/Ca and REE/F ratios with the La, Ce, Pr, and 529 Nd and some of the HREE (i.e., Dy, Y, and Ho) plotting below the stoichiometric line. Clear positive REE/Ca and REE/F ratios can be observed for 531 the experiments conducted at the highest temperature of 250 °C. We interpret these trends to indicate the possible precipitation of LREE fluorides, 533 particularly at mildly acidic conditions, and precipitation of mostly HREE 534 depleted secondary fluorite at the higher experimental temperature. These observations are in line with the calculated saturation indices for La- and Cefluoride for the mildly acidic solutions (Supplementary Materials, Appendix 537 B3) as well as their chondrite-normalized REE profiles. The latter display 538 a depletion in La, Ce, Pr, and Nd over adjacent LREE such as Sm and Eu (Fig. 9b), which is less pronounced in the alkaline solutions.

Overall these trends indicate that in alkaline solutions there is a higher potential for REE fluoride precipitation, whereas in the acidic solutions the measured REE mostly correspond to stoichiometric dissolution from fluorite and possibly the precipitation of secondary LREE-depleted/Y-enriched fluorite. While the mass balance calculations permit identifying the potential formation of secondary REE-bearing minerals, the measured variations in F concentrations are too small to affect the calculated fluorite solubility products, i.e. mildly acidic and alkaline solutions plot close to the fluorite saturation line (Fig. 7).

50 4.3. Controls of aqueous speciation on REE mobility

The mobility of REE in natural hydrothermal fluids depends on the stability of REE complexes and the solubility of REE-bearing minerals. In

critical mineral deposits with acidic/mildly acidic fluids, chlorides and sulfates are considered major transporting ligands of REE, whereas fluorides
and phosphates are considered depositional ligands due to the low solubility
of fluorides and phosphates (Migdisov and Williams-Jones, 2014; Gysi et al.,
2018). In near-neutral to alkaline solutions, the REE hydroxyl and/or carbonate complexes could potentially become important (Pourtier et al., 2010;
Perry and Gysi, 2018; Louvel et al., 2022; Nisbet et al., 2022).

The speciation of REE was calculated using the GEMS code package (Ku-560 lik et al., 2013) to determine the dominant aqueous complexes controlling the 561 solubility of REE in the experiments. Figure 12 shows an example of pre-562 dominant (mole fractions) species for Ce (i.e., LREE) and Er (i.e., HREE) 563 as a function of temperature, pH and salinity. In the NaCl-free experiments (Fig. 12a-b), the REE fluoride complexes are calculated to be predominant in both acidic and mildly acidic solutions, and the REE hydroxyl complexes in alkaline solutions. The dominant REE fluoride species include ${\rm REEF^{2+}},$ and REEF $_2^+$ at 100–150 °C with the appearance of REECl $^{2+}$ in the acidic 568 and REE hydroxyl complexes (i.e., REEOH $^{2+}$ and REE(OH) $^{+}_{2}$) in the mildly acidic solutions at 250 °C. In the alkaline experimental solutions, REE(OH)⁰₃ and $\text{REE}(\text{OH})_4^-$ are predominant between 100–250 °C. Experiments con-571 ducted in NaCl solutions yield a significant increase in the calculated stability of REE chloride over the REE fluoride complexes, in both, acidic and mildly acidic solutions (Fig. 12c). This is particularly pronounced for the Ce species, for which, the fluoride complexes are negligible between 100–250 °C. 576

Here we carried out an additional series of acid/base titration simula-

577

tions using the GEMS code package to show the overall predicted stability of aqueous REE species and saturation of REE fluorides and hydroxides at 579 150 °C for a REE-bearing fluid in equilibrium with fluorite at pH of 2 to 10. Figure 13 illustrates the calculated pH-log a_{REE} diagram using currently 581 available experimental data for REE aqueous complexes at 150 °C for a fluid 582 saturated with fluorite and using the updated solubility products retrieved 583 in our study (Table 5). In the simulations with no NaCl (Fig. 13a,c), the 584 solubility of REE is controlled by the formation of REE fluorides and the formation of REE fluoride species at pH values between 2-6.5 and the solubility of REE hydroxides and stability of REE hydroxyl complexes at pH 587 values above 5.5–6.5. The predominance of REE fluoride complexes in the 588 simulated acidic fluids is different from the observations by Migdisov and Williams-Jones (2014) who did not consider the availability of fluoride from fluorite dissolution in their model. Addition of 15 wt.% NaCl (Fig. 13b,d) 591 increases the stability of REE chloride complexes, which predominate for Ce 592 but not for Er. Further addition of chloride increases the predominance of REE chloride species, in agreement with the simulations by Migdisov and Williams-Jones (2014). The present simulations highlight the importance of considering additional sources and sinks of F⁻ for REE mobility, which includes the solubility of fluorite and the formation of fluoride complexes such as NaF⁰ (Eq. 8), which affect the solubility of REE-bearing fluoride minerals. Thermodynamic modeling of REE mobility in F-rich natural systems is 599 still hampered by several limitations that need to be pointed out. Simulated REE speciation in F-bearing hydrothermal fluids by Migdisov and Williams-Jones (2014) suggest that REE chloride complexes are primarily responsible

for the transport of REE in these fluids. In contrast to REE chloride, fluoride, and sulfate complexes for which thermodynamic properties are determined 604 experimentally (Migdisov et al., 2009), our knowledge about the stability of 605 REE hydroxyl and carbonate complexes is currently limited to the thermodynamic data derived by Haas et al. (1995). The latter have a high degree 607 of uncertainty (Migdisov et al., 2016). Only a few experimental studies have 608 been conducted recently on the REE speciation at near-neutral to alkaline 609 conditions (e.g. Wood et al., 2002; Louvel et al., 2022). However, solubility 610 experiments and molecular dynamic simulations are missing for those species 611 and would be needed. 612

The formation of REE fluorides, such as fluocerite, is rather uncommon 613 in natural systems but can be a precursor to more stable REE minerals 614 (Strzelecki et al., 2022). Instead, fluorocarbonates (i.e., bastnäsite, parisite, synchysite, etc.) are commonly found in magmatic-hydrothermal critical 616 mineral deposits including alkaline complexes and carbonatites (Smith et al., 617 2000; Williams-Jones et al., 2000; Gysi and Williams-Jones, 2013; Gysi et al., 618 2016; Wu et al., 2021; Beard et al., 2022; Patel et al., 2022; Verplanck et al., 619 2022). However, thermodynamic properties that permit modeling the stability of these minerals are still scarce (Gysi and Williams-Jones, 2015; Shivaramaiah et al., 2016; Voigt et al., 2016; Goncharov et al., 2022). Further, 622 these simulations commonly use a set amount of REE added to the fluid to calculate REE speciation. The primary control of fluorite solubility on the mobility of the REE (Eq. 13) has until now not been predicted even though it is a common vein mineral in many REE mineral deposits where hydrothermal overprint has been documented (Smith and Henderson, 2000;

Smith et al., 2000; Samson et al., 2004; Gysi and Williams-Jones, 2013; Gysi et al., 2016).

5. Conclusions

In this experimental study we quantify the combined effects of pH, salinity 631 and temperature on REE mobility upon fluorite dissolution at temperatures 632 >100 °C. A major finding from the experiments is that the solubility of REE can be enhanced in alkaline solutions with the addition of NaCl, with concentrations in the fluids reaching similar levels to the acidic solutions (i.e., 635 NaCl-free and NaCl solutions). The processes affecting REE mobility in-636 vestigated here include the role of: 1) fluorite solubility; 2) aqueous REE 637 speciation; 3) precipitation of secondary REE fluorides and REE-depleted fluorite under hydrothermal conditions. Fluorite reaction textures in conjunction with fluid chemistry were investigated in detail and indicate that the experiments represent a dissolution-controlled environment. Further, we derived a series of new fluorite solubility constants based on the experiments between 150 and 254 °C that match with previous low temperature solubility studies. The experiments also indicate that the Supert92 database overpredicts fluorite solubility between 25 and 250 °C.

Upon approach to equilibrium with fluorite, and in the absence of doping
the experimental solutions with 0.5 ppm REE, the affinity to form secondary
REE minerals was found to be generally low, except for the lighter REE
(i.e., La, Ce, Pr, and Nd). The fluorite solubility was found to be controlled
dominantly by the formation of Ca chloride and hydroxyl species, NaF⁰,
and the association behavior of HF⁰ (Eqs. 5-8). The overall REE mobility
behavior is controlled by fluid chemistry (pH and salinity). The maximum

REE concentrations in the fluid range between $\sim 1 \times 10^{-5}$ and 1×10^{-7} mol/kg, and minimum concentrations between $\sim 1 \times 10^{-9}$ and 1×10^{-11} mol/kg (Table 4), with the highest concentrations found in the NaCl-bearing solutions (indpendent of pH) and the lowest concentrations in the alkaline NaCl-free solutions.

Based on a series of mass balance equations (Eqs. 15-16), the following conclusions can be made: 1) acidic fluid produces a REE signature that behaves stoichiometric with fluorite; 2) mildly acidic and alkaline fluids promote the formation of REE-depleted fluorite; 3) addition of NaCl promotes increased fluorite dissolution and saturation with secondary LREE fluorides.

There is a need for high temperature precipitation experiments to study the REE incorporation mechanisms into hydrothermal fluorite, similar to the recent study by Perry and Gysi (2020) on REE-doped calcite. These next steps will allow deriving a thermodynamic solid solution model to simulate the mobility of REE and predict REE signatures in hydrothermal fluorite veins.

Acknowledgments

This project was supported by the National Science Foundation to APG (NSF CAREER grant EAR-2039674). We would like to thank B. Frey, D. Baca and H. Han from the New Mexico Bureau of Geology and Mineral Resources, New Mexico Tech Geochemistry laboratory, for assistance on the IC, ICP-OES and ICP-MS instruments. J. Thompson from the U.S. Geological Survey Federal Center in Denver, Colorado, provided assistance on the LA-ICP-MS instrument. K. Pfaff and K. Livingston provided assistance with

- scanning electron microscope imaging in the Mineral and Materials Charac-
- terization Facility in the Department of Geology and Geological Engineering,
- 679 Colorado School of Mines. We are grateful for access to the Surprise mine in
- New Mexico, and thank P. Simmons and his team for guidance in the field and
- 681 for allowing us to collect fluorite crystals in the mine. This manuscript ben-
- efited greatly from the constructive reviews by M. Louvel and O. Vasyukova.
- We also thank Editor-in-Chief M. Böttcher for handling this manuscript.

684 References

- Aries, S., Valladon, M., Polvé, M., Dupré, B., 2000. A routine method for
- oxide and hydroxide interference corrections in ICP-MS chemical analysis
- of environmental and geological samples. Geostandards Newsletter 24,
- 688 19–31.
- Beard, C.D., Goodenough, K.M., Borst, A.M., Wall, F., Siegfried, P.R.,
- Deady, E.A., Pohl, C., Hutchison, W., Finch, A.A., Walter, B.F., Elliott,
- H.A., Brauch, K., 2022. Alkaline-Silicate REE-HFSE Systems. Economic
- Geology doi:https://doi.org/10.5382/econgeo.4956.
- 693 Betkowski, W.B., Harlov, D.E., Rakovan, J.F., 2016. Hydrothermal mineral
- replacement reactions for an apatite-monazite assemblage in alkali-rich flu-
- ids at 300-600 °C and 100 MPa. American Mineralogist 101, 2620–2637.
- 696 Blundy, J., Wood, B., 1994. Prediction of crystal-melt partition coefficients
- from elastic moduli. Nature 372, 452–454.
- Blundy, J., Wood, B., 2003. Partitioning of trace elements between crystals
- and melts. Earth and Planetary Science Letters 210, 383–397.

- Curti, E., Kulik, D.A., Tits, J., 2005. Solid solutions of trace Eu(III) in calcite: Thermodynamic evaluation of experimental data over a wide range of pH and pCO₂. Geochimica et Cosmochimica Acta 69, 1721–1737.
- Diakonov, I.I., Ragnarsdottir, V.K., Tagirov, B.R., 1998. Standard thermo-
- dynamic properties and heat capacity equations of rare earth hydroxides:
- 705 II. Ce(III)-, Pr-, Sm-, Eu(III)-, Gd-, Tb-, Dy-, Ho-, Er-, Tm-, Yb-, and Y-
- hydroxides. Comparison of thermochemical and solubility data. Chemical
- ⁷⁰⁷ Geology 151, 327–347.
- Elliott, H.A., Wall, F., Chakhmouradian, A.R., Siegfried, P.R., Dahlgren, S.,
- Weatherley, S., Finch, A.A., Marks, M.A., Dowman, E., Deady, E., 2018.
- Fenites associated with carbonatite complexes: A review. Ore Geology
- 711 Reviews 93, 38–59.
- Frenkel, M., Kabo, G.J., Marsh, K.N., Roganov, G.N., Wilhoit, R.C., 1994.
- Thermodynamics of organic compounds in the gas state. TRC Data Series,
- Vol. I, College Station, TX.
- Gagnon, J.E., Samson, I.M., Fryer, B.J., Williams-Jones, A.E., 2003. Com-
- positional heterogeneity in fluorite and the genesis of fluorite deposits:
- Insights from LA-ICP-MS analysis. Canadian Mineralogist 41, 365–382.
- Garand, A., Mucci, A., 2004. The solubility of fluorite as a function of
- ionic strength and solution composition at 25 °C and 1 atm total pressure.
- 720 Marine Chemistry 91, 27–35.
- Goncharov, V.G., Nisbet, H., Strzelecki, A.C., Benmore, C.J., Migdisov,

- A.A., Xu, H., Guo, X., 2022. Energetics of hydroxylbastnäsite solid solu-
- tions, $La_{1-x}Nd_xCO_3OH$. Geochimica et Cosmochimica Acta 330, 47–66.
- Goodenough, K.M., Wall, F., Merriman, D., 2018. The rare earth elements:
- Demand, global resources, and challenges for resourcing future generations.
- Natural Resources Research 27, 201–216.
- Guillong, M., Meier, D., Allan, M., Heinrich, C., Yardley, B., 2008. SILLS:
- A MATLAB-based program for the reduction of laser ablation ICP-MS
- data of homogeneous materials and inclusions. Mineralogical Association
- of Canada Short Course Vol. 40, Vancouver, B.C. pp. 328–333.
- Gysi, A.P., 2017. Numerical simulations of CO₂ sequestration in basaltic
- rock formations: challenges for optimizing mineral-fluid reactions. Pure
- and Applied Chemistry 89, 24–29.
- Gysi, A.P., Harlov, D., Miron, G.D., 2018. The solubility of monazite
- (CePO₄), SmPO₄, and GdPO₄ in aqueous solutions from 100 to 250 °C.
- Geochimica et Cosmochimica Acta 242, 143–164.
- Gysi, A.P., Harlov, D.E., 2021. Hydrothermal solubility of TbPO₄, HoPO₄,
- TmPO₄, and LuPO₄ xenotime endmembers at pH of 2 and temperatures
- between 100 and 250 °C. Chemical Geology 567, 120072.
- 740 Gysi, A.P., Williams-Jones, A.E., 2013. Hydrothermal mobilization of
- pegmatite-hosted REE and Zr at Strange Lake, Canada: A reaction path
- model. Geochimica et Cosmochimica Acta 122, 324–352.
- 743 Gysi, A.P., Williams-Jones, A.E., 2015. The thermodynamic properties of
- bastnäsite-(Ce) and parisite-(Ce). Chemical Geology 392, 87–101.

- Gysi, A.P., Williams-Jones, A.E., Collins, P., 2016. Lithogeochemical vectors
 for hydrothermal processes in the Strange Lake peralkaline granitic REE Zr-Nb deposit. Economic Geology 111, 1241–1276.
- Haas, J.R., Shock, E.L., Sassani, D.C., 1995. Rare earth elements in hydrothermal systems: Estimates of standard partial molal thermodynamic properties of aqueous complexes of the rare earth elements at high pressures and temperatures. Geochimica et Cosmochimica Acta 59, 4329–4350.
- Harlov, D.E., Meighan, C.J., Kerr, I.D., Samson, I.M., 2016. Mineralogy,
 chemistry, and fluid-aided evolution of the Pea Ridge Fe Oxide-(Y + REE)
 deposit, Southeast Missouri, USA. Economic Geology 111, 1963–1984.
- Harlov, D.E., Wirth, R., Förster, H.J., 2005. An experimental study of
 dissolution–reprecipitation in fluorapatite: fluid infiltration and the formation of monazite. Contributions to Mineralogy and Petrology 150, 268–286.
- Harlov, D.E., Wirth, R., Hetherington, C.J., 2011. Fluid-mediated partial
 alteration in monazite: The role of coupled dissolution-reprecipitation in
 element redistribution and mass transfer. Contributions to Mineralogy and
 Petrology 162, 329–348.
- Hatch, G.P., 2012. Dynamics in the global market for rare earths. Elements 8, 341–346.
- Helgeson, H.C., Kirkham, D.H., Flowers, G.C., 1981. Theoretical prediction
 of the thermodynamic behavior of aqueous electrolytes by high pressures

- and temperatures; IV, calculation of activity coefficients, osmotic coeffi-
- cients, and apparent molal and standard and relative partial molal prop-
- erties to 600 °C and 5kb. American Journal of Science 281, 1249–1516.
- Henry, R.L., 2018. Low temperature aqueous solubility of fluorite at tem-
- peratures of 5, 25, and 50 °C and ionic strengths up to 0.72 M. Master's
- thesis. Colorado School of Mines.
- Johnson, J.W., Oelkers, E.H., Helgeson, H.C., 1992. SUPCRT92: A software
- package for calculating the standard molal thermodynamic properties of
- minerals, gases, aqueous species, and reactions from 1 to 5000 bar and 0
- to 1000 °C. Computers & Geosciences 18, 899–947.
- Kolonin, G., Shironosova, G., 2002. Thermodynamic model for REE com-
- plexation in the course of interaction between REE-fluorite and hydrother-
- mal fluid. Geochemistry International 40, 103–112.
- 780 Kulik, D.A., Wagner, T., Dmytrieva, S.V., Kosakowski, G., Hingerl, F.F.,
- Chudnenko, K.V., Berner, U.R., 2013. GEM-Selektor geochemical model-
- ing package: Revised algorithm and GEMS3K numerical kernel for coupled
- simulation codes. Computational Geosciences 17, 1–24.
- Kurovskaya, N.A., Malinin, S.D., 1983. The solubility of CaF₂ in aqueous
- CaCl₂-HCl-NaCl solutions at 25-200 °C and determination of CaF₂ activity
- product. Geochemistry International 20, 13–27.
- Longerich, H.P., Jackson, S.E., Günther, D., 1996. Inter-laboratory note.
- laser ablation inductively coupled plasma mass spectrometric transient

- signal data acquisition and analyte concentration calculation. Journal of
- Analytical Atomic Spectrometry 11, 899–904.
- Louvel, M., Etschmann, B., Guan, Q., Testemale, D., Brugger, J., 2022.
- Carbonate complexation enhances hydrothermal transport of rare earth
- elements in alkaline fluids. Nature Communications 13, 1–11.
- McDonough, W., Sun, S.s., 1995. The composition of the Earth. Chemical
 Geology 120, 223–253.
- Migdisov, A.A., Williams-Jones, A.E., 2014. Hydrothermal transport and
- deposition of the rare earth elements by fluorine-bearing aqueous liquids.
- Mineralium Deposita 49, 987–997.
- Migdisov, A.A., Williams-Jones, A.E., Brugger, J., Caporuscio, F.A., 2016.
- 800 Hydrothermal transport, deposition, and fractionation of the REE: Ex-
- perimental data and thermodynamic calculations. Chemical Geology 439,
- 802 13-42.
- Migdisov, A.A., Williams-Jones, A.E., Wagner, T., 2009. An experimental
- study of the solubility and speciation of the Rare Earth Elements (III)
- in fluoride- and chloride-bearing aqueous solutions at temperatures up to
- 300 °C. Geochimica et Cosmochimica Acta 73, 7087–7109.
- Miron, G., Wagner, T., Kulik, D., Lothenbach, B., 2017. An internally
- consistent thermodynamic dataset for aqueous species in the system Ca-
- Mg-Na-K-Al-Si-O-H-C-Cl to 800 °C and 5 kbar. American Journal of
- Science 317, 755–806.

- Miron, G.D., Kulik, D.A., Dmytrieva, S.V., Wagner, T., 2015. GEMSFITS:
- Code package for optimization of geochemical model parameters and in-
- verse modeling. Applied Geochemistry 55, 28–45.
- Miron, G.D., Wagner, T., Kulik, D.A., Heinrich, C.A., 2016. Inter-
- nally consistent thermodynamic data for aqueous species in the system
- Na-K-Al-Si-O-H-Cl. Geochimica et Cosmochimica Acta 187, 41-78.
- Möller, P., Bau, M., Dulski, P., Lüders, V., 1998. REE and yttrium frac-
- tionation in fluorite and their bearing on fluorite formation, in: Proc 9th
- Quadrennial IAGOD Symposium, E. Schweizerbart'sche Verlagsbuchand-
- lung, Stuttgart, Germany. pp. 575–592.
- Nadoll, P., Rehm, M., Duschl, F., Klemd, R., Kraemer, D., Sósnicka, M.,
- 2018. REY and trace element chemistry of fluorite from post-variscan
- hydrothermal veins in paleozoic units of the North German Basin. Geo-
- sciences (Switzerland) 8, 1–29. doi:10.3390/geosciences8080283.
- Navrotsky, A., Lee, W., Mielewczyk-Gryn, A., Ushakov, V.S., Anderko, A.,
- Wu, H., Riman, R.E., 2015. Thermodynamics of solid phases containing
- rare earth oxides. The Journal of Chemical Thermodynamics 88, 126–141.
- Nisbet, H., Migdisov, A., Goncharov, V., van Hinsberg, V., Williams-Jones,
- A., Xu, H., Guo, X., 2022. The solubility and speciation of Nd in
- carbonate-bearing hydrothermal fluids up to 250 °C. Chemical Geology
- 831 , 121122.
- Nordstrom, D.K., 2022. Evaluation for internal consistency in the thermody-

- namic network involving fluorite, cryolite and villiaumite solubilities and aqueous species at 25 °C and 1 bar. Mineralogical Magazine 86, 652–660.
- Nordstrom, D.K., Jenne, E.A., 1977. Fluorite solubility equilibria in selected geothermal waters. Geochimica et Cosmochimica Acta 41, 175–188.
- North, R., Tuff, M., 1986. Fluid-inclusion and trace-element analyses of some barite-fluorite deposits in south-central New Mexico, in: Clemons, R., King, W., Mack, G., Zidek, J. (Eds.), New Mexico Geological Society Guidebook, 37th Annual Fall Field Conference Guidebook. Truth or Consequences Region, pp. 301–306.
- Patel, A.K., Mishra, B., Upadhyay, D., Pruseth, K.L., 2022. Mineralogical and geochemical evidence of dissolution-reprecipitation controlled hydrothermal rare earth element mineralization in the Amba Dongar Carbonatite Complex, Gujarat, Western India. Economic Geology 117, 683–702.
- Perry, E., Gysi, A.P., 2018. Rare earth elements in mineral deposits: Speciation in hydrothermal fluids and partitioning in calcite. Geofluids 2018.
- Perry, E., Gysi, A.P., 2020. Hydrothermal calcite-fluid REE partitioning experiments at 200 °C and saturated water vapor pressure. Geochimica et Cosmochimica Acta 286, 177–197.
- Pourtier, E., Devidal, J.L., Gibert, F., 2010. Solubility measurements of synthetic neodymium monazite as a function of temperature at 2 kbars, and aqueous neodymium speciation in equilibrium with monazite. Geochimica et Cosmochimica Acta 74, 1872–1891.

- Proust, P., Vera, J.H., 1989. PRSV: The Stryjek-Vera modification of the
- Peng-Robinson equation of state. parameters for other pure compounds
- of industrial interest. The Canadian Journal of Chemical Engineering 67,
- 858 170–173.
- Putnis, C.V., Putnis, A., 2022. A mechanism of ion exchange by interface-
- coupled dissolution-precipitation in the presence of an aqueous fluid. Jour-
- nal of Crystal Growth, 126840.
- Richardson, C.K., Holland, H.D., 1979. The solubility of fluorite in hy-
- drothermal solutions, an experimental study. Geochimica et Cosmochimica
- 864 Acta 43, 1313–1325.
- Robie, R.A., Hemingway, B.S., 1995. Thermodynamic properties of minerals
- and related substances at 298.15 K and 1 bar (10⁵ Pascals) pressure and
- at higher temperatures. U.S. Geological Survey Bulletin 2131.
- Robinson, R., Stokes, R., 1968. Electrolyte solutions. Butterworths, London.
- 869 Salvi, S., Williams-Jones, A.E., 1990. The role of hydrothermal processes in
- the granite-hosted Zr, Y, REE deposit at Strange Lake, Quebec/Labrador:
- Evidence from fluid inclusions. Geochimica et Cosmochimica Acta 54,
- 2403-2418.
- 873 Samson, I.M., Wood, S.A., Finucane, K., 2004. Fluid inclusion characteristics
- and genesis of the fluorite-parisite mineralization in the Snowbird Deposit,
- Montana. Economic Geology 99, 1727–1744.
- 876 Schönenberger, J., Köhler, J., Markl, G., 2008. REE systematics of fluorides,

- calcite and siderite in peralkaline plutonic rocks from the Gardar Province,
- South Greenland. Chemical Geology 247, 16–35.
- Schwinn, G., Markl, G., 2005. REE systematics in hydrothermal fluorite.
- 880 Chemical Geology 216, 225–248.
- Shannon, R.D., 1976. Revised effective ionic radii and systematic studies of
- interatomic distances in halides and chalcogenides. Acta crystallographica
- section A: crystal physics, diffraction, theoretical and general crystallogra-
- phy 32, 751–767.
- Shivaramaiah, R., Anderko, A., Riman, R.E., Navrotsky, A., 2016. Ther-
- modynamics of bastnaesite: A major rare earth ore mineral. American
- 887 Mineralogist 101, 1129–1134.
- 888 Shock, E.L., Helgeson, H.C., 1988. Calculation of the thermodynamic and
- transport properties of aqueous species at high pressures and temperatures:
- 890 Correlation algorithms for ionic species and equation of state predictions
- to 5 kb and 1000 °C. Geochimica et Cosmochimica Acta 52, 2009–2036.
- Shock, E.L., Oelkers, E.H., Johnson, J.W., Sverjensky, D.A., Helgeson, H.C.,
- 1992. Calculation of the thermodynamic properties of aqueous species at
- high pressures and temperatures. Effective electrostatic radii, dissociation
- constants and standard partial molal properties to 1000 °C and 5 kbar.
- Journal of the Chemical Society, Faraday Transactions 88, 803–826.
- Shock, E.L., Sassani, D.C., Willis, M., Sverjensky, D.A., 1997. Inorganic
- species in geologic fluids: Correlations among standard molal thermody-

- namic properties of aqueous ions and hydroxide complexes. Geochimica et
- 900 Cosmochimica Acta 61, 907–950.
- 901 Simmons, P., 2019. Cookes Peak Mining District, Luna County, New Mexico.
- 902 Rocks & Minerals 94, 214–239.
- 903 Smith, M., Campbell, L., Kynicky, J., 2015. A review of the genesis of the
- world class bayan obo fe-ree-nb deposits, inner mongolia, china: Mul-
- tistage processes and outstanding questions. Ore Geology Reviews 64,
- 906 459-476.
- 907 Smith, M.P., Henderson, P., 2000. Preliminary fluid inclusion constraints
- on fluid evolution in the Bayan Obo Fe-REE-Nb deposit, inner Mongolia,
- 909 China. Economic Geology 95, 1371–1388.
- 910 Smith, M.P., Henderson, P., Campbell, L.S., 2000. Fractionation of the REE
- during hydrothermal processes: constraints from the Bayan Obo Fe-REE-
- Nb deposit, Inner Mongolia, China. Geochimica et Cosmochimica Acta
- 913 64, 3141–3160.
- 914 Stryjek, R., Vera, J.H., 1986. PRSV: An improved Peng—Robinson equa-
- tion of state for pure compounds and mixtures. The Canadian Journal of
- chemical Engineering 64, 323–333.
- 917 Strzelecki, A.C., Migdisov, A., Boukhalfa, H., Sauer, K., McIntosh, K.G.,
- Currier, R.P., Williams-Jones, A.E., Guo, X., 2022. Fluocerite as a pre-
- cursor to rare earth element fractionation in ore-forming systems. Nature
- 920 Geoscience 15, 327–333.

- 921 Strübel, G., 1965. Untersuchungen über die hydrothermal Löslichkeit von 922 Flusspat (CaF₂). Geologische Rundschau 3, 83–95.
- 923 Sverjensky, D.A., Shock, E.L., Helgeson, H.C., 1997. Prediction of the ther-
- modynamic properties of aqueous metal complexes to 1000 °C and 5 kb.
- Geochimica et Cosmochimica Acta 61, 1359–1412.
- Tanger, J.C., Helgeson, H.C., 1988. Calculation of the thermodynamic and
- transport properties of aqueous species at high pressures and temperatures;
- revised equations of state for the standard partial molal properties of ions
- and electrolytes. American Journal of Science 288, 19–98.
- 930 Tropper, P., Manning, C.E., 2007. The solubility of fluorite in H₂O and
- H₂O-NaCl at high pressure and temperature. Chemical Geology 242, 299-
- 932 306.
- Van Hinsberg, V., Migdisov, A.A., Williams-Jones, A.E., 2010. Reading the
- mineral record of fluid composition from element partitioning. Geology 38,
- 935 847-850.
- Vasyukova, O.V., Williams-Jones, A.E., 2018. Direct measurement of metal
- concentrations in fluid inclusions, a tale of hydrothermal alteration and
- 938 REE ore formation from Strange Lake, Canada. Chemical Geology 483,
- 939 385–396.
- Vasyukova, O.V., Williams-Jones, A.E., 2019. Closed system fluid-mineral-
- mediated trace element behaviour in peralkaline rare metal pegmatites:
- Evidence from Strange Lake. Chemical Geology 505, 86–99.

- Verplanck, P.L., Farmer, G.L., Kettler, R.M., Lowers, H.A., Johnson, C.A.,
- Koenig, A.E., Blessington, M.J., 2022. Petrogenesis and rare earth element
- mineralization of the Elk Creek carbonatite, Nebraska, USA. Ore Geology
- 946 Reviews 146, 104953.
- Voigt, M., Rodriguez-Blanco, J.D., Vallina, B., Benning, L.G., Oelkers, E.H.,
- ⁹⁴⁸ 2016. An experimental study of hydroxylbastnasite solubility in aqueous
- solutions at 25 °C. Chemical Geology 430, 70–77.
- 950 Wagner, T., Kulik, D.A., Hingerl, F.F., Dmytrieva, S.V., 2012. GEM-
- 951 Selektor geochemical modeling package: TSolMod library and data in-
- terface for multicomponent phase models. The Canadian Mineralogist 50,
- 953 1173-1195.
- Walter, B.F., Giebel, R.J., Steele-MacInnis, M., Marks, M.A., Kolb, J.,
- Markl, G., 2021. Fluids associated with carbonatitic magmatism: A criti-
- cal review and implications for carbonatite magma ascent. Earth-Science
- 957 Reviews 215, 103509.
- 958 Williams-Jones, A., Samson, I., Olivo, G., 2000. The genesis of hydrothermal
- 959 fluorite-REE deposits in the Gallinas Mountains, New Mexico. Economic
- 960 Geology 95, 327–341.
- Wood, S.A., Palmer, D.A., Wesolowski, D.J., Benezeth, P., 2002. The aque-
- ous geochemistry of the rare earth elements and yttrium. Part XI. The
- solubility of Nd(OH)₃ and hydrolysis of Nd³⁺ from 30 to 290 °C at satu-
- rated water vapor pressure with in-situ pH_m measurement. Water-Rock

- Interaction, Ore Deposits, and Environmental Geochemistry: A Tribute to
- David A. Crerar, Geochemical Society Special Publication 7. pp. 229–256.
- 967 Wu, M., Samson, I.M., Qiu, K., Zhang, D., 2021. Concentration mecha-
- nisms of rare earth element-Nb-Zr-Be mineralization in the Baerzhe de-
- posit, Northeast China: Insights from textural and chemical features of
- amphibole and rare metal minerals. Economic Geology 116, 651–679.
- ⁹⁷¹ Zhang, W., Zhou, L., Tang, H., Li, H., Song, W., Xie, G., 2017. The solubility
- of fluorite in Na-K-Cl solutions at temperatures up to 260 °C and ionic
- 973 strengths up to 4 mol/kg H₂O. Applied Geochemistry 82, 79–88.

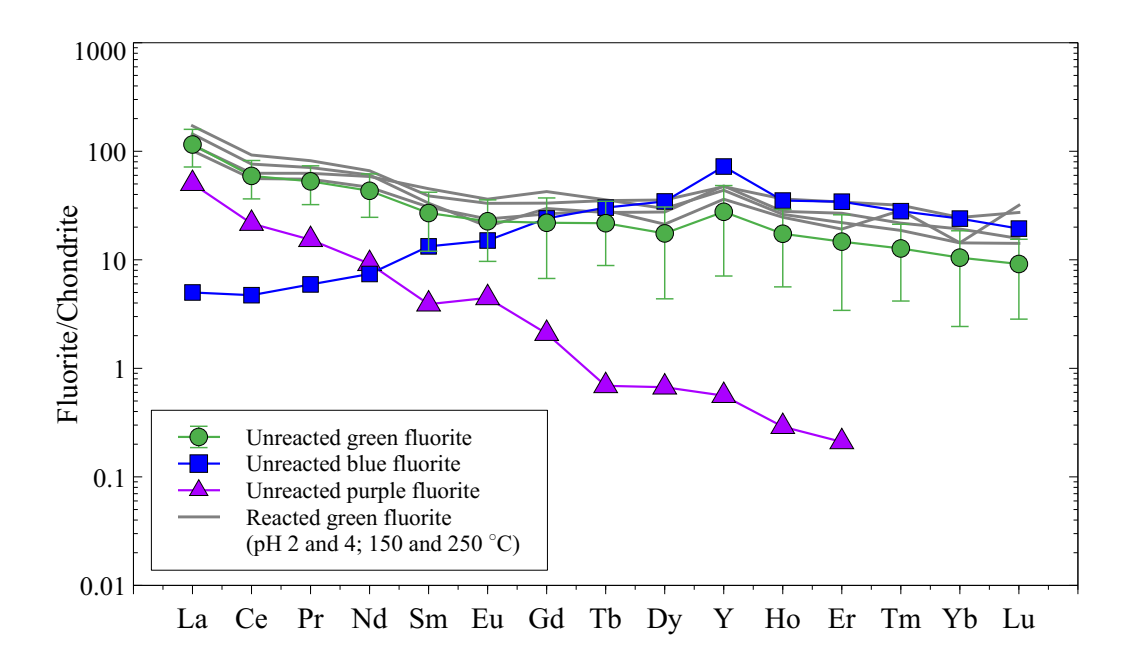


Figure 1: Chondrite-normalized (McDonough and Sun, 1995) fluorite composition measured using LA-ICP-MS and showing the mean REE profiles of the three different unreacted fluorite types and reacted green fluorite. The error bars for the green fluorite represent the standard deviation of the mean and indicate that the fluorite reacted rims with the REE doped experimental solutions displays limited variability in comparison to the core-to-rim variability observed in the unreacted fluorite. The full dataset is available in the Supplementary Materials (Tables A1 and A2).

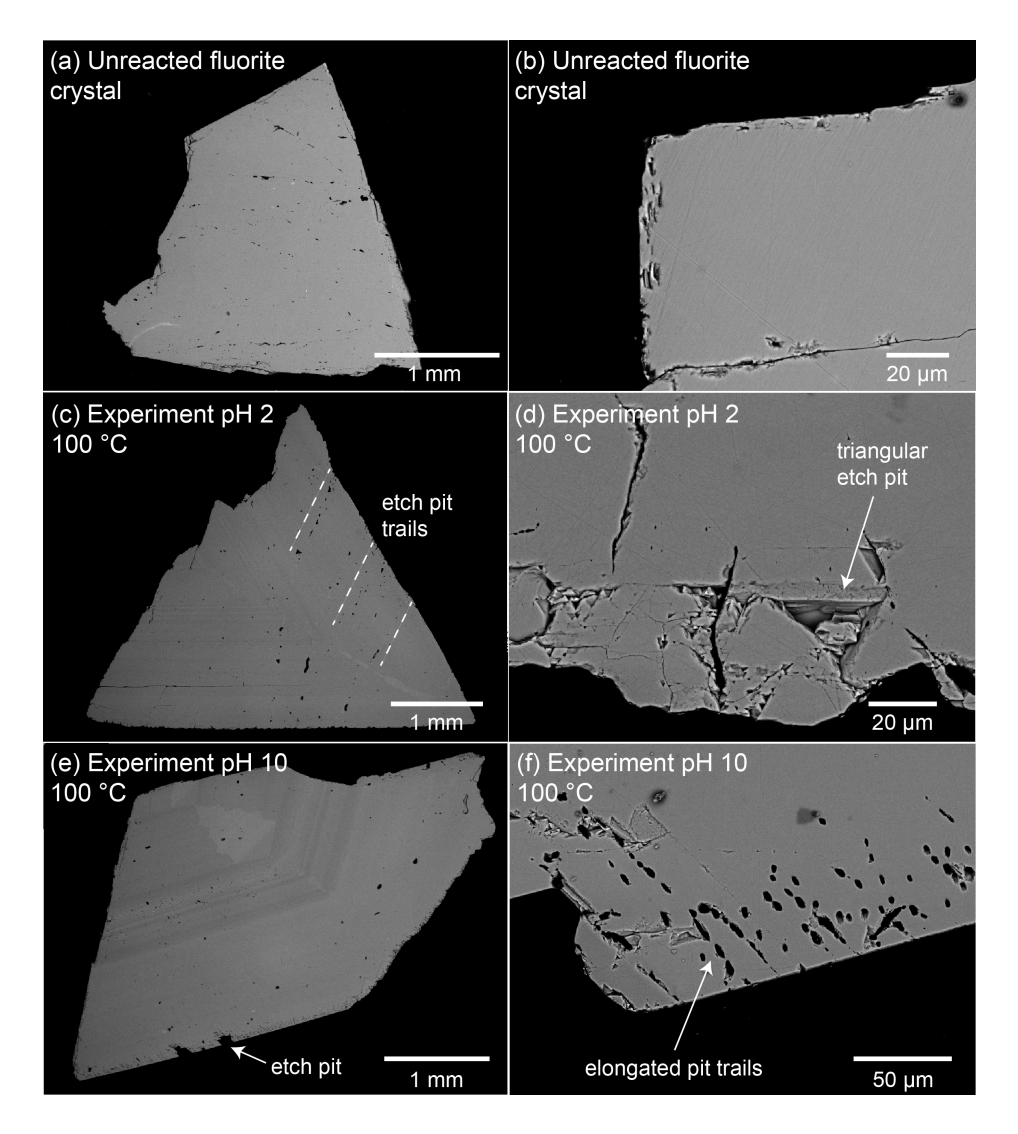


Figure 2: Backscattered electron images of unreacted and reacted fluorite crystal fragments presented as a function of starting pH of the experimental solutions. Overviews (a, c, e) and magnified views (b, d, f) are shown for each reaction texture. (a-b) Unreacted fluorite crystals display slight etching on the surface from crystal cleaning. (c-d) Fluorite crystals reacted with acidic solutions (pH 2) exhibit increased pitting in the crystal, leaching along crystal edges, and the formation of triangular etch pits along cleavage planes. (e-f) Fluorite crystals reacted with alkaline solutions (pH 10) exhibit dissolution networks \sim 50-100 µm and elongated pit trails. Starting experimental conditions are listed in Table 2, and additional images for the pH 4 experiments are found in the Supplementary Materials (Appendix B).

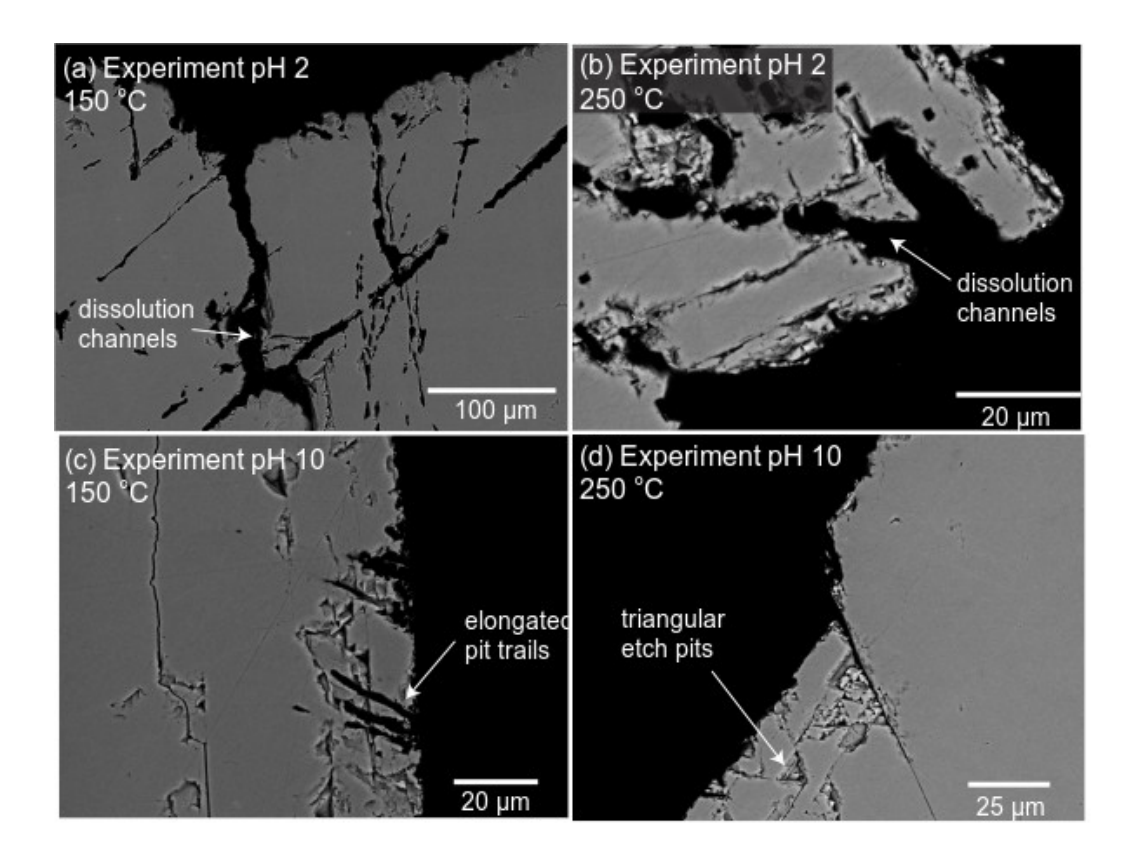


Figure 3: Backscattered electron images showing reacted fluorite crystal surfaces presented as a function of pH and experimental temperature of 150 and 250 °C. (a-b) Fluorite crystals reacted with acidic solutions (pH 2) display the formation of dissolution channels along cleavage planes and irregular leached crystal surfaces. (c-d) Fluorite crystals reacted with alkaline solutions (pH 10) display the formation of elongated pits trails along the crystal edges and the formation of triangular etch pits near the crystal edges. Dissolution textures are generally more pronounced with increased temperature in comparison to the 100 °C experiments (Fig. 2). Starting experimental conditions are listed in Table 2.

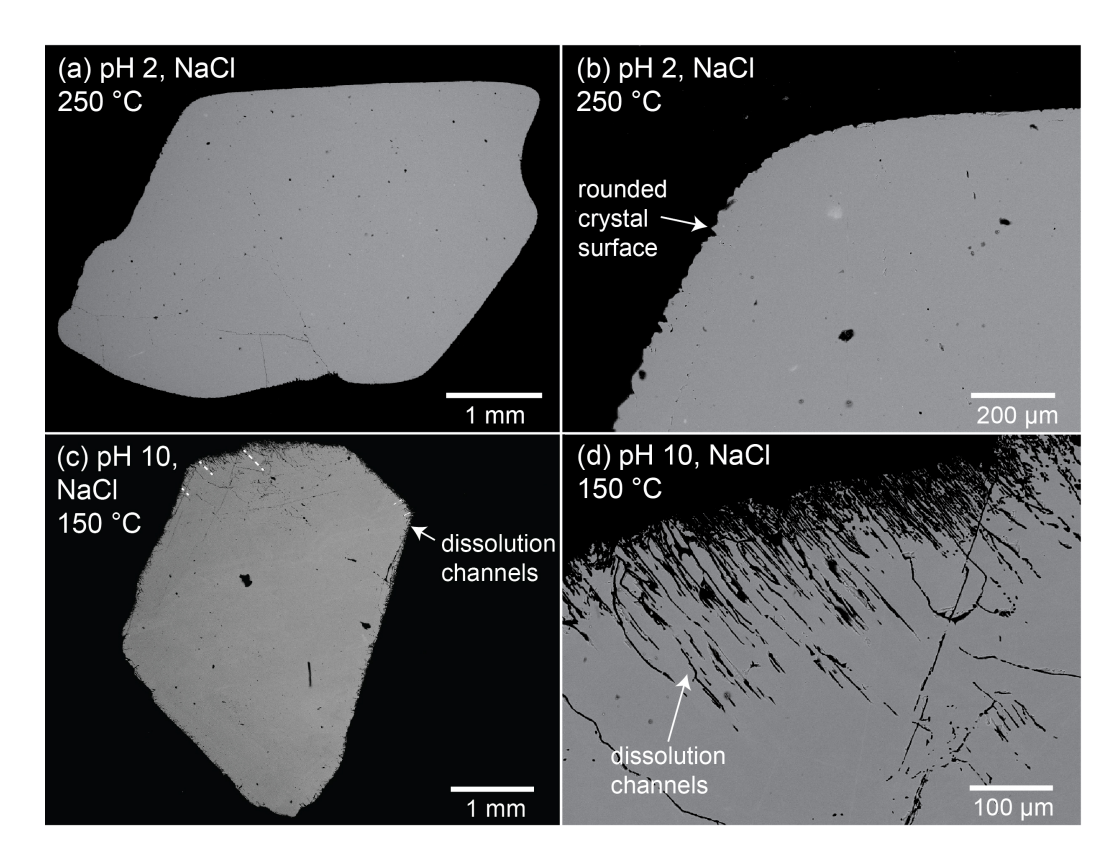


Figure 4: Backscattered electron images of fluorite crystal fragments reacted with saline (~15 wt.% NaCl) solutions with acidic (a-b) and alkaline (c-d) pH. (a-b) Addition of NaCl to acidic solutions (pH 2) results in increased intensity of fluorite dissolution textures with the development of leached rounded crystal surfaces. (c-d) Addition of NaCl to the alkaline solutions (pH 10) results in the development of >100 μm dissolution channels along cleavage planes. Starting experimental conditions are listed in Table 2.

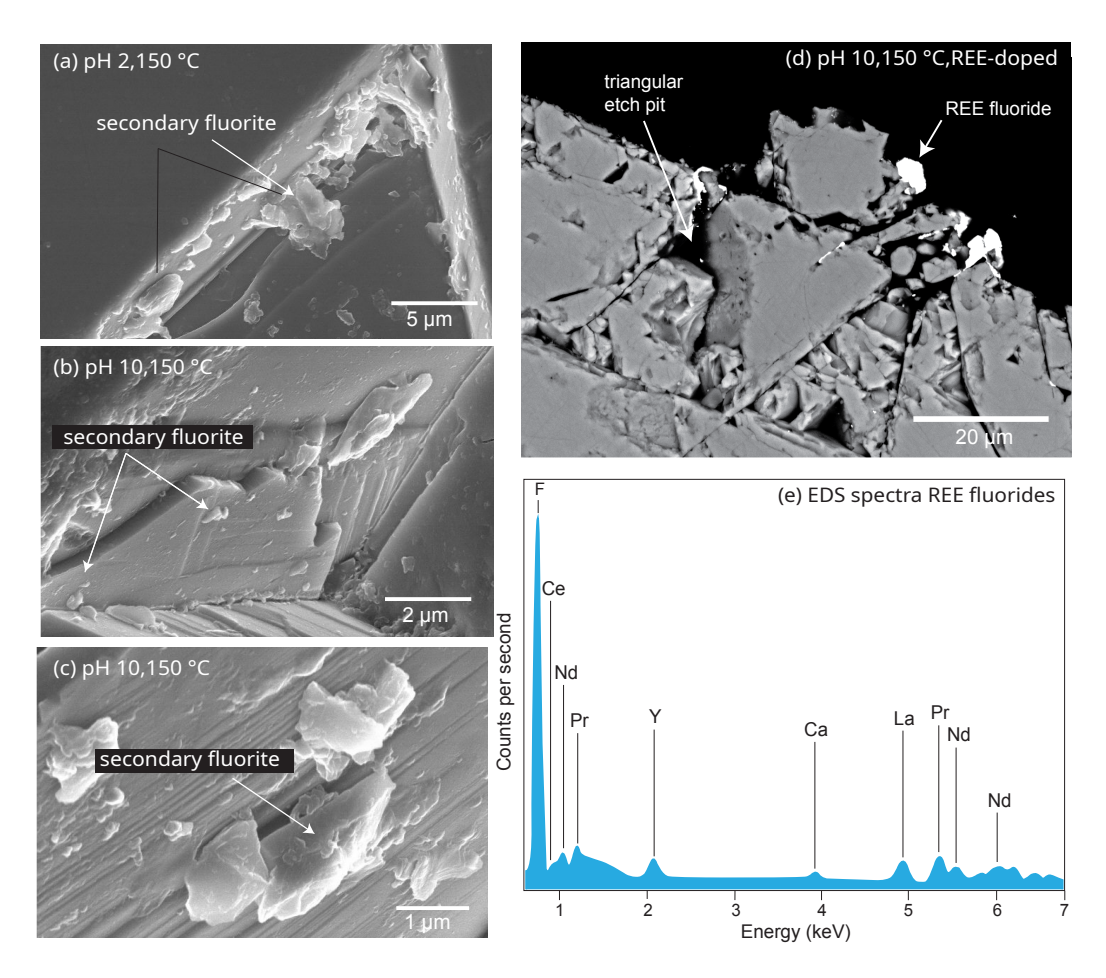


Figure 5: Scanning electron and BSE images of secondary minerals formed. (a-c) Small fluorite precipitates formed on the reacted fluorite surfaces. (d) BSE image and (e) SEM-EDS spectra of secondary REE fluorides precipitated on the fluorite crystal surface and along cleavage planes and etch pits formed in the REE doped (0.5 ppm) experiments conducted in mildly acidic (pH 4) solutions and a temperature of 250 °C. EDS spectra indicate the presence of the La, Ce, Pr, Nd, Y and F with minimal Ca.

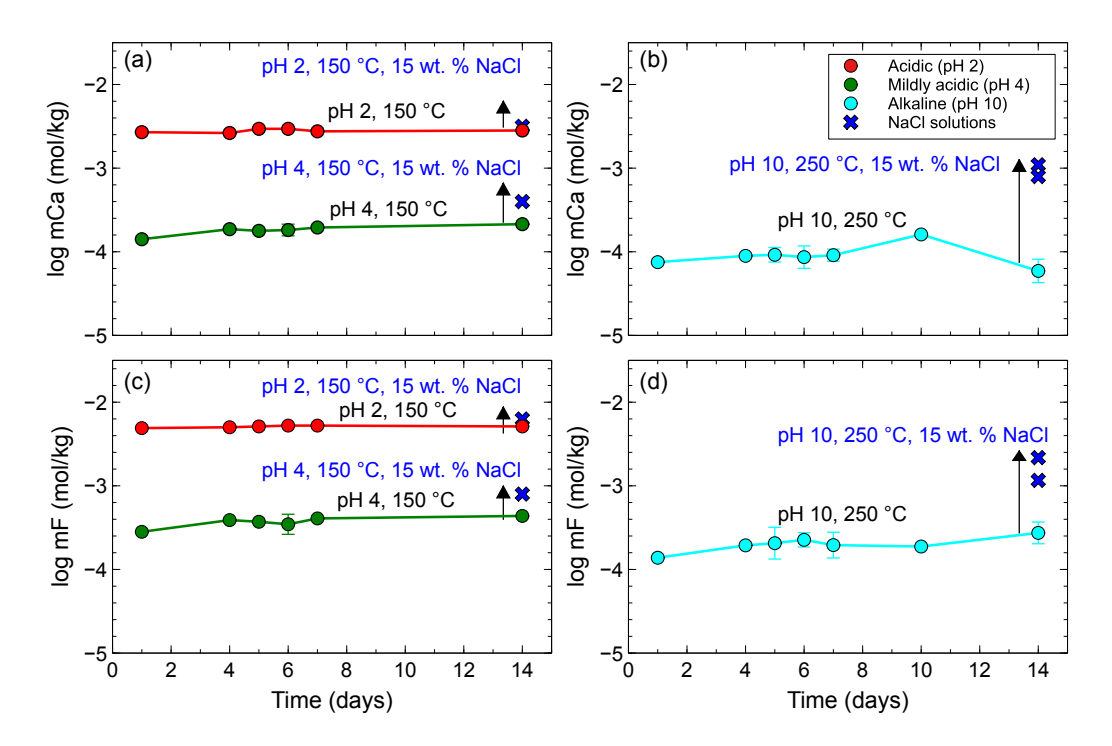


Figure 6: Kinetic experiments showing the logarithm of total dissolved Ca and F molalities (mol/kg) in the quenched experimental solutions as a function of time for experiments in acidic solutions and mildly acidic solutions at 150 °C (a, c), and for experiments in alkaline solutions at 250 °C (b, d). Addition of \sim 15 wt.% NaCl results in increased fluorite dissolution at each experimental condition (blue symbols). Error bars indicate the standard deviation (1 σ) determined from duplicate experiments.

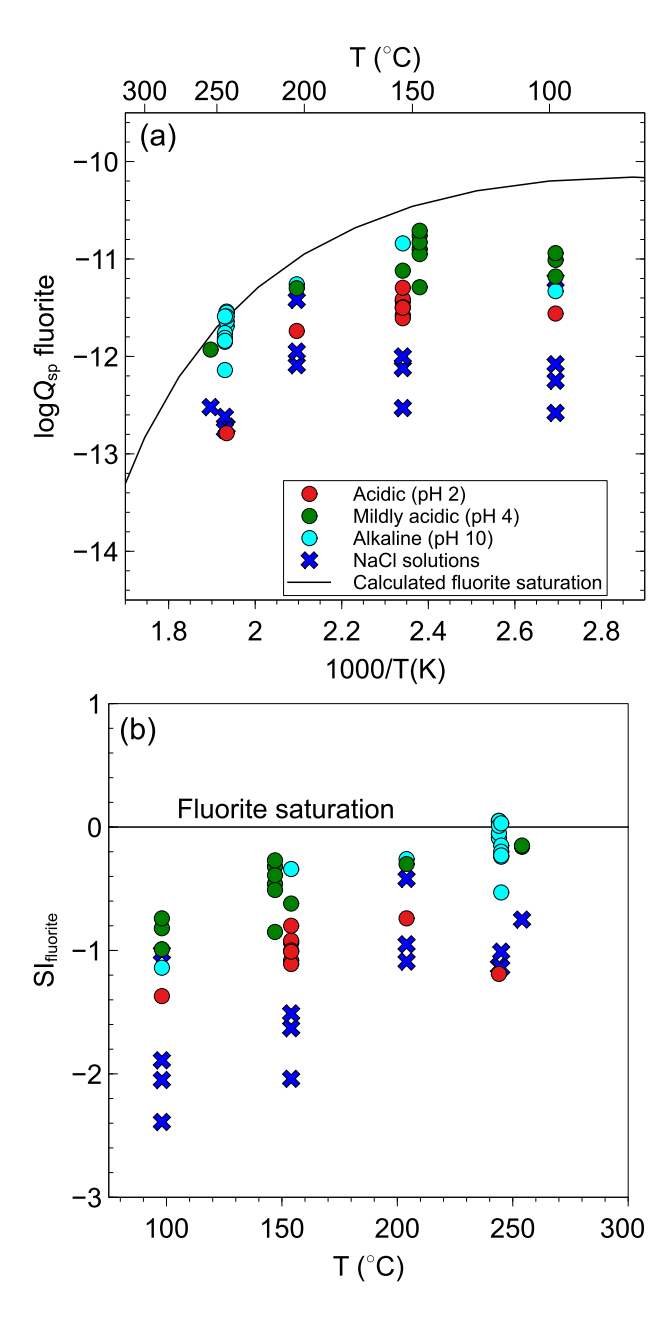


Figure 7: (a) Logarithm of fluorite solubility products $(Q_{\rm sp})$ and (b) fluorite saturation index (SI) as a function of temperature for experiments conducted in acidic, mildly acidic and alkaline solutions. Fluorite saturation was calculated using thermodynamic properties from Robie and Hemingway (1995) for fluorite, from Miron et al. (2017) for Ca^{2+} , and Supert92 and for F^- . Calculated activities of aqueous species are found in the Supplementary Materials (Table A4).

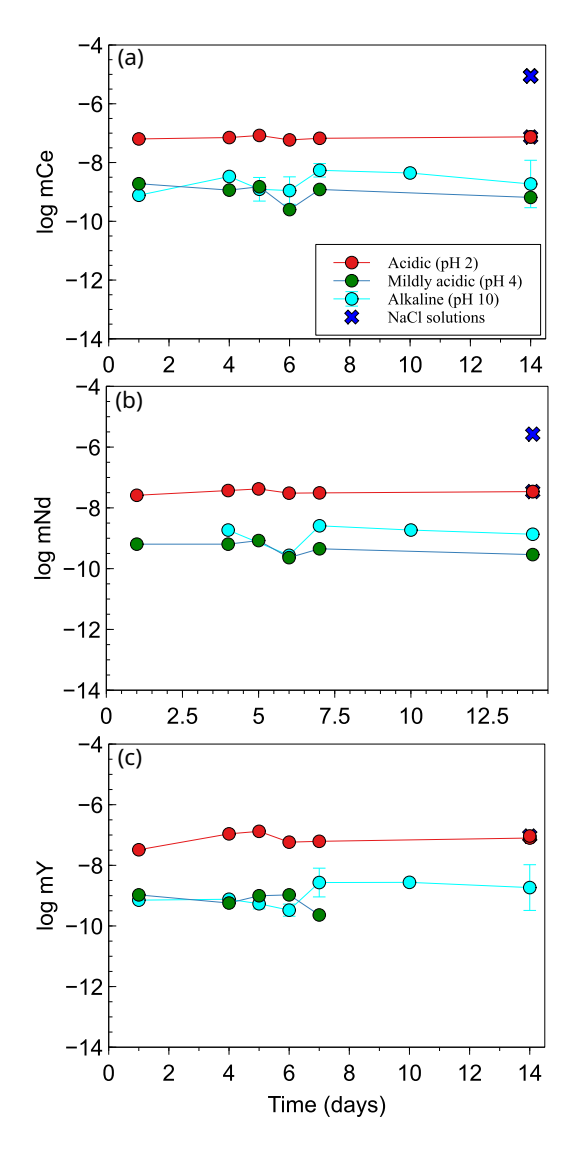


Figure 8: Kinetic experiments showing typical REE concentrations (mol/kg) in the quenched experimental solutions as a function of reaction time with fluorite. Experiments in acidic (pH 2) and mildly acidic (pH 4) solutions were conducted at 150 °C and experiments in alkaline (pH 10) solutions at 250 °C. Addition of \sim 15 wt.% NaCl to the experiments (blue dots) led to an overall increase in dissolved REE concentrations. Error bars indicate the standard deviation (1σ) determined from duplicate experiments.

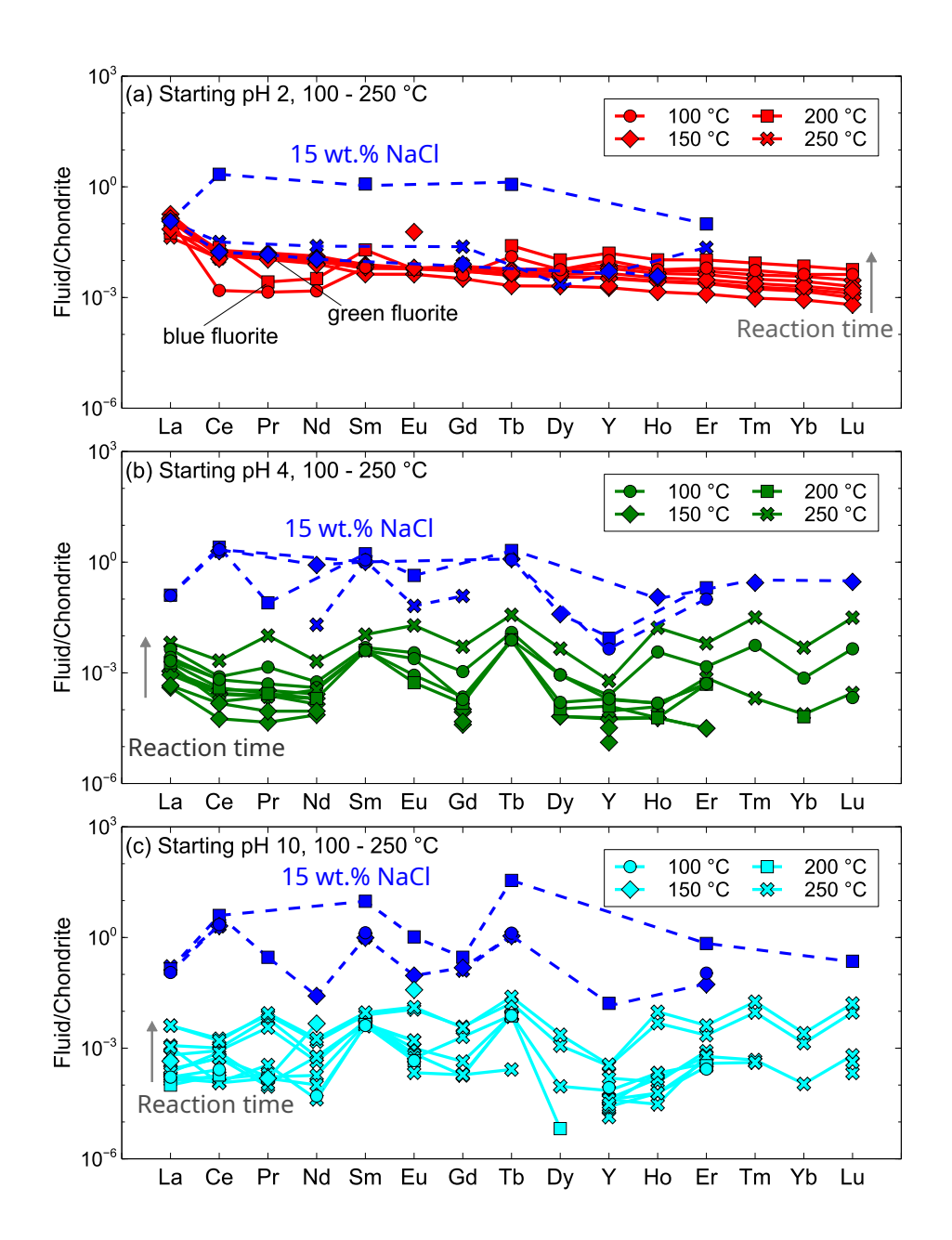


Figure 9: Chondrite-normalized REE concentrations measured in quenched solutions using ICP-MS. Rare earth elements distribution in (a) acidic solutions (pH 2), (b) mildly acidic solutions (pH 4), and (c) alkaline solutions (pH 10). Reaction time indicates experiments quenched after 1 to 14 days, and shows an increase in REE concentrations when reaching steady-state concentrations.

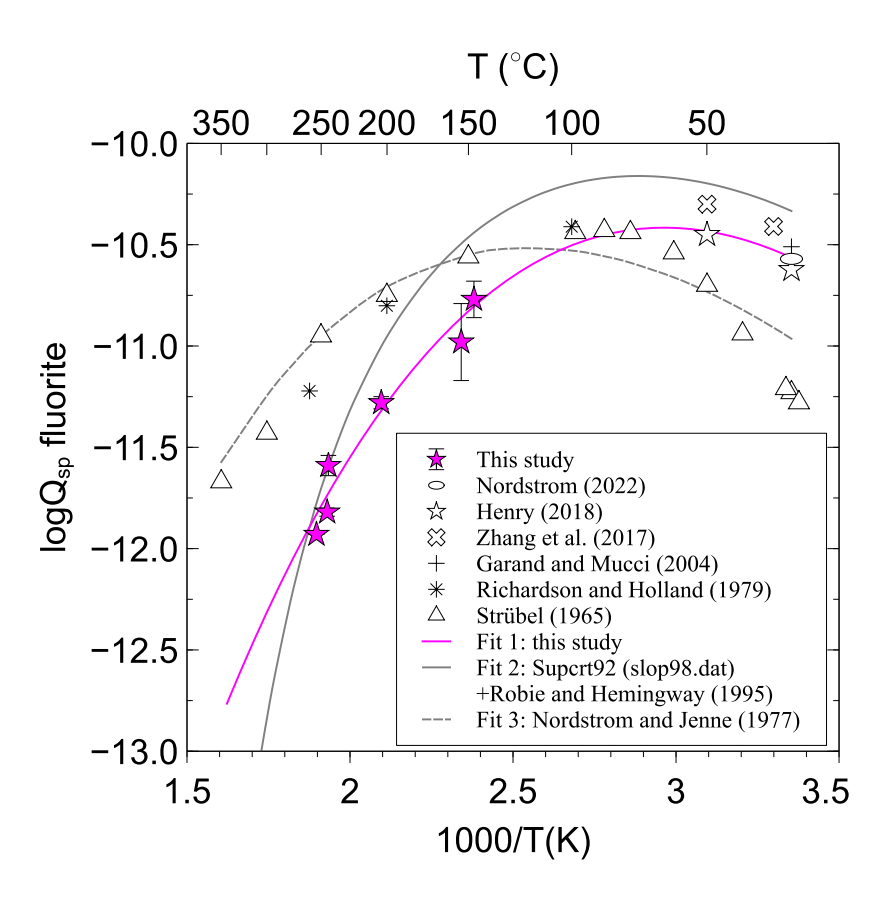


Figure 10: Fluorite solubility products $(\log Q_{sp})$ as a function of temperature showing a comparison of the experimental data from this study with other data sources (Supplementary Materials, Table A6). Fit 1 includes experimental solubility data between 150–250 °C from this study and data between 25–50 °C from Henry (2018) and Garand and Mucci (2004), and data at 100 °C from Richardson and Holland (1979); fitted parameters are listed in Table 5. Fit 2 was calculated using the properties of Ca²⁺ and F⁻ from Sucprt92, slop98.dat dataset (Sverjensky et al., 1997) and optimized by Miron et al. (2017), and fluorite properties from Robie and Hemingway (1995). Fit 3 was calculated from the parameters listed in Nordstrom and Jenne (1977).

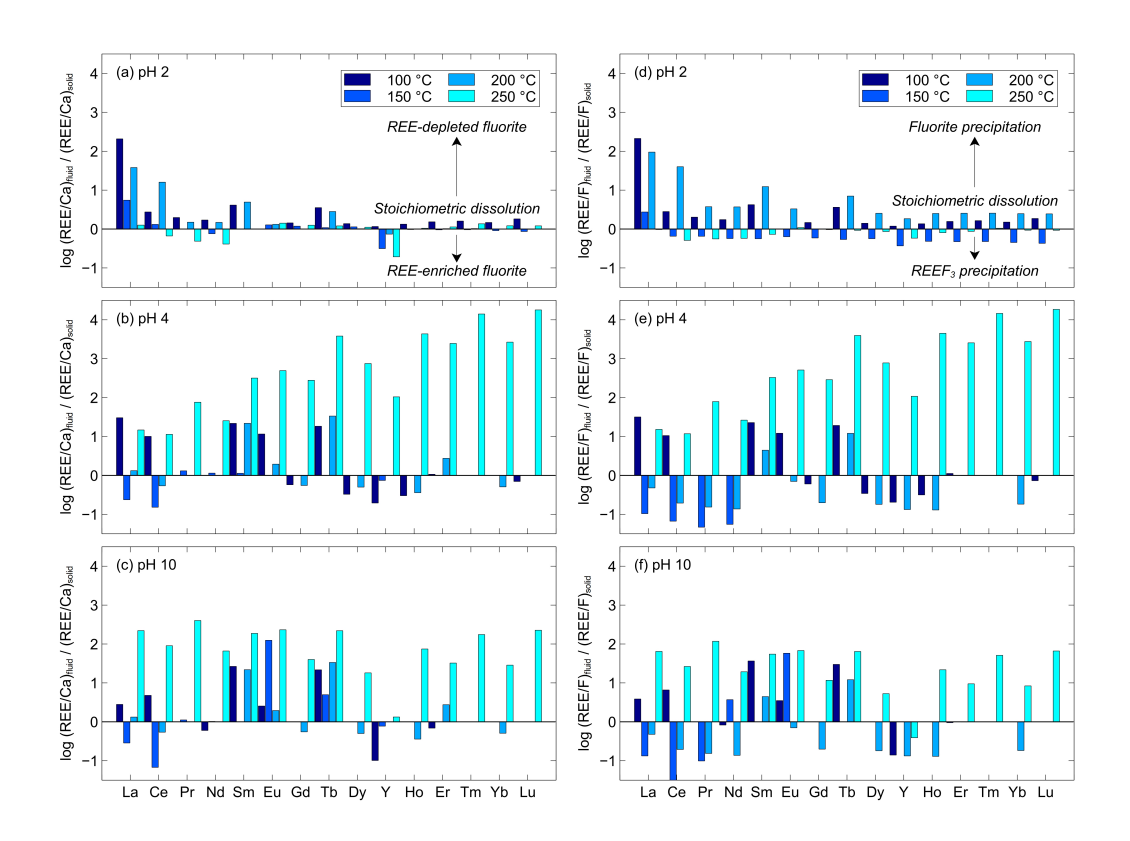


Figure 11: Mass balance calculations used to estimate the REE partitioning behavior between fluid and fluorite in experiments not doped with REE. Logarithm of (a-c) REE/Ca and (d-f) REE/F ratios were calculated from the REE concentrations measured in the fluorite and the quenched experimental solutions (Tables 1 and 3–4). Values above the stoichiometric dissolution line (i.e. ratios of 0) indicate an affinity for the precipitation of secondary REE-depleted fluorite. Values below the stoichiometric dissolution line indicate an affinity for the precipitation of either REE-enriched fluorite (a-c) or REE fluorides (d-f). The full dataset of calculated ratios can be found in the Supplementary Materials (Table A5).

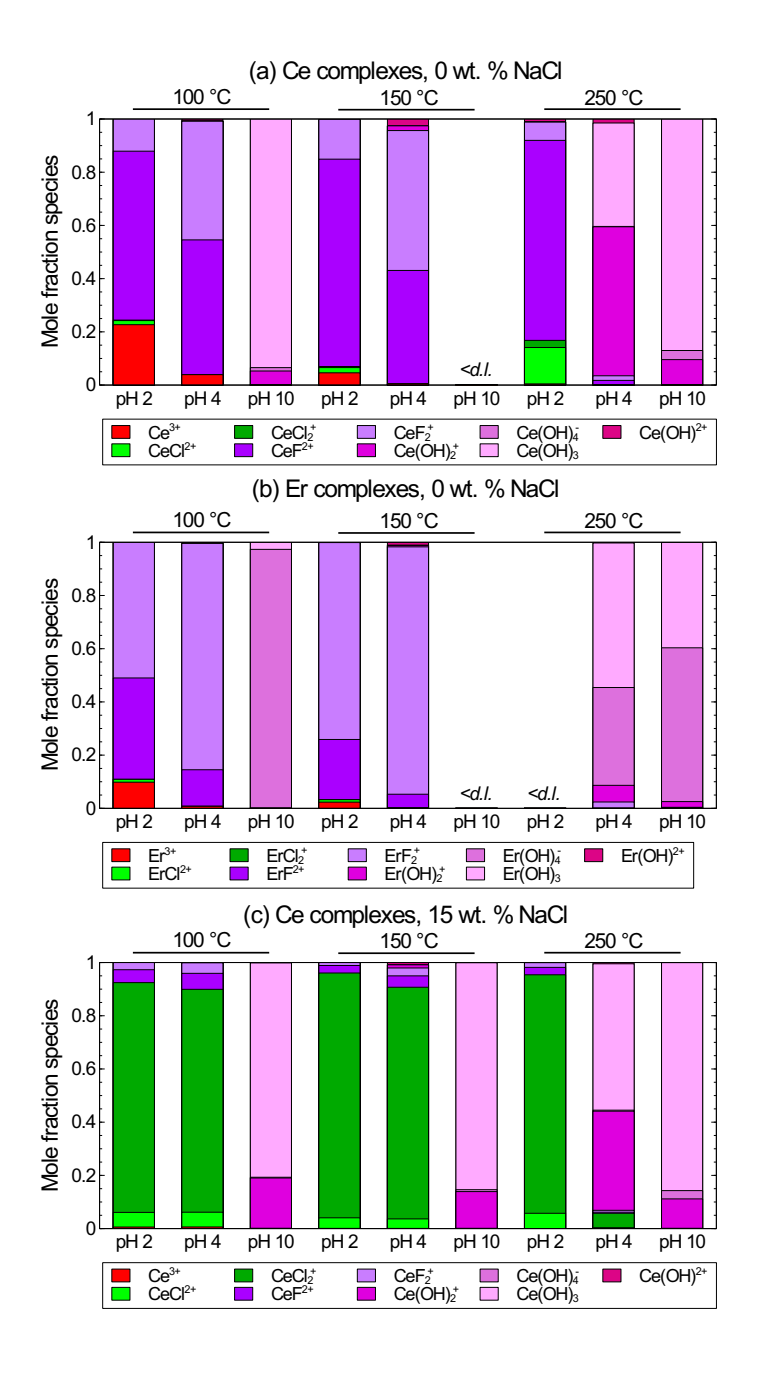


Figure 12: Cumulative mole fractions of stable Ce and Er aqueous species at the different experimental conditions. (a-b) Speciation calculated in the NaCl-free experiments. (c) Speciation calculated in the NaCl solutions. The full dataset of calculated REE species activities can be found in the Supplementary Materials (Table A4).

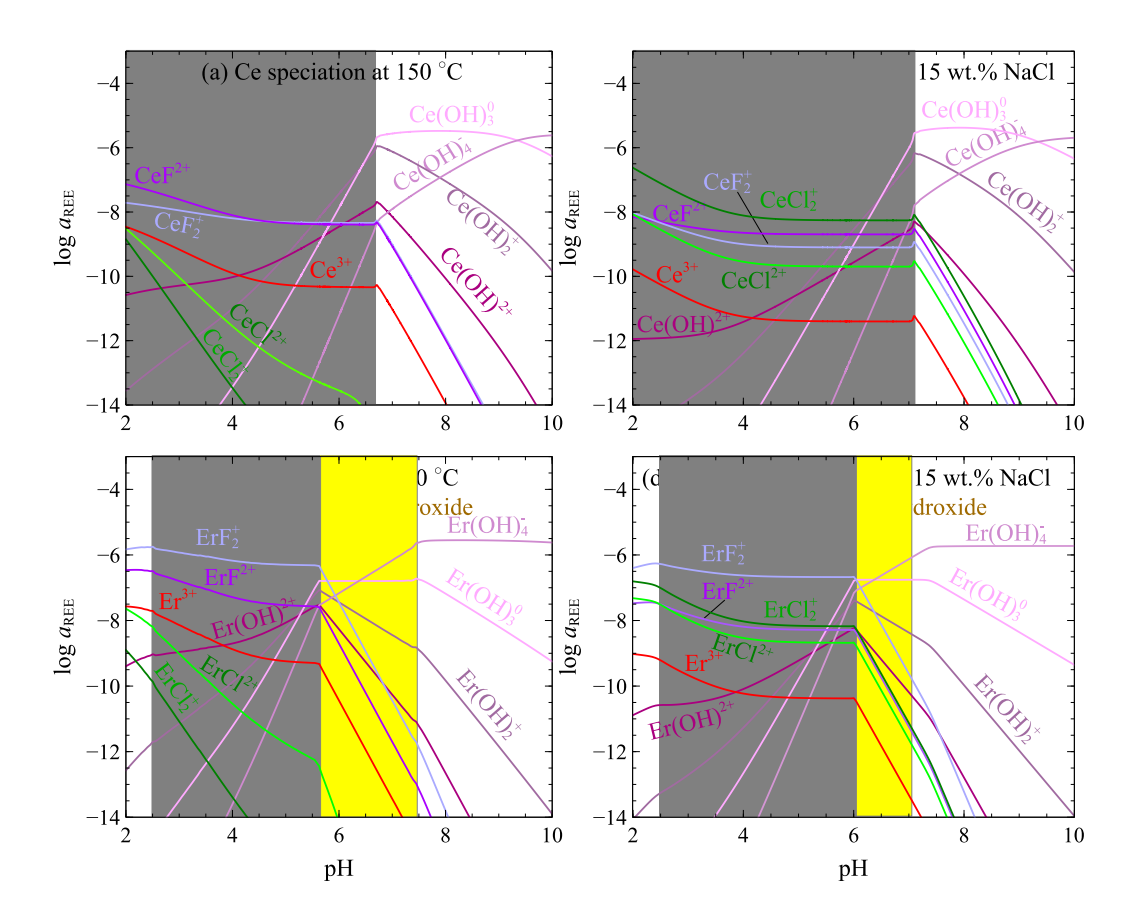


Figure 13: Modeled REE speciation diagrams at 150 °C showing the calculated logarithm activities of aqueous REE species in equilibrium with fluorite as a function of pH and starting salinity. The modeled fluid compositions (1000 g $\rm H_2O$, 0–0.05 m $\rm HCl$, 0–0.06 m NaOH, 0.5 ppm REE, 0 and 15 wt.% NaCl) were equilibrated with 5 g fluorite at pH values of 2 to 10 using the GEMS code package and an inverse titration model. Also shown are the stability fields for REE minerals (fluoride in grey shade and hydroxide in yellow shade).

Table 1: LA-ICP-MS data (in ppm) of unreacted fluorite crystals (green, blue, and purple) from the Cooke's Peak mining district, New Mexico. Mean values and standard deviations (1σ) represent variation across fluorite crystal core to rim profiles. The full dataset can be found as Supplementary Materials, Table A1.

	Green		Blue		Purple		d.l.
	(n = 104)	1σ	(n = 60)	1σ	(n = 10)	1σ	
Na (ppm)	8.5	3.8	19	14	8.4	1.1	0.6
Mg	7.8	6.2	13	8	5.7	0.8	0.03
Si	211	59	323	96	210	32	26
P	2.9	1.0	52	49	2.9	0.7	1.8
Sr	25	7.3	32	14	26	2	0.005
Y	43	32	114	75	1.0	0.5	0.003
La	27	10	1.2	1.2	12	2	0.003
Се	36	14	2.9	2.3	13	2	0.002
Pr	4.9	1.9	0.6	0.4	1.4	0.3	0.001
Nd	20	9	3.4	2.0	4.2	1.1	0.005
Sm	4.0	2.2	2.0	1.0	0.6	0.2	0.007
Eu	1.3	0.7	0.8	0.4	0.3	0.1	0.005
Gd	4.4	3.0	4.8	2.4	0.4	0.2	0.01
Tb	0.8	0.5	1.1	0.6	d.l.	-	0.05
Dy	4.3	3.2	8.5	4.8	0.2	0.1	0.002
Но	0.9	0.6	1.9	1.1	0.03	0.01	0.003
Er	2.4	1.8	5.5	3.4	0.05	0.02	0.002
Tm	0.3	0.2	0.7	0.5	d.l.	-	0.002
Yb	1.7	1.3	3.9	2.7	0.03	0.02	0.002
Lu	0.2	0.2	0.5	0.4	d.l.	-	0.006
∑La-Lu	109	-	38	-	32	-	-

n = the number of spots measured; d.l. = detection limit

Table 2: Starting conditions of the fluorite solubility experiments. Starting pH values (pH $_{25^{\circ}C}$) were close to 2 (acidic), 4 (mildly acidic), and 10 (alkaline) at room temperature, with some solutions initially doped with \sim 15 wt. % NaCl and 0.5 ppm REE.

		Exp	T	Time	$\mathrm{pH}_{25} \circ C$	$\log m HCl$	$\log m \mathrm{NaOH}$	$\log m \text{NaCl}$	REE
			(°C)	(days)		(mol/kg)	(mol/kg)	(mol/kg)	(ppm)
Acidic (pH 2)	blue	28	98	14	1.97	-1.97	-	-	-
NaCl	green	40	98	14	1.98	-1.98	-	0.36	-
	green	003A-F	154	1 to 14	1.98	-1.98	-	-	-
	green	5	154	14	1.97	-1.97	-	-	-
NaCl	green	7	154	14	1.98	-1.97	-	0.33	-
REE doped	green	15	154	14	1.99	-1.89	-2.58	-	0.5
	green	34	204	14	1.97	-1.97	-	-	-
NaCl	blue	37	204	14	1.98	-1.98	-	0.34	-
	green	10	244	14	1.97	-1.97	-	-	-
NaCl	green	12	244	14	1.98	-1.98	-	0.36	-
REE doped	green	20	245	14	1.99	-1.89	-2.58	-	0.5
Mildly acidic (pH 4)	green	42	98	14	3.94	-3.94	-	-	-
	blue	29	98	14	4.05	-4.05	-	-	-
	${\rm green}^a$	33	98	14	4.05	-4.05	-	-	-
NaCl	blue	31	98	14	4.05	-4.05	-	0.34	-
	green	001A-F	147	1 to 14	4.05	-4.05	-	-	-
	green	19	154	6	4.05	-4.05	-	-	-
NaCl	green	17	154	14	4.05	-4.05	-	0.36	-
	green	35	204	14	3.94	-3.94	-	-	-
NaCl	blue	38	204	14	4.05	-4.05	-	-	-
REE doped	green	21	245	14	2.99	-1.93	-1.97	-	0.5

NaCl	green	22	245	14	4.05	-4.05	-	0.38	-
	${\rm green}^a$	25	254	14	4.05	-4.05	-	-	-
	green	26	254	14	4.05	-4.05	-	-	-
Alkaline (pH 10)	blue	30	98	14	10.07	-	-3.93	-	-
NaCl	blue	32	98	14	10.07	-	-3.93	0.34	-
NaCl	green	41	98	14	10.07	-	-3.93	0.34	-
	green	6	154	14	10.07	-	-3.93	-	-
NaCl	green	18	154	14	10.07	-	-3.93	0.36	-
	${\rm green}^a$	36	204	14	10.07	-	-3.93	-	-
NaCl	blue	39	204	14	10.07	-	-3.93	0.37	-
	green	043A-D	244	$1\ \rm to 10$	10.07	-	-3.93	-	-
	green	11	244	14	10.07	-	-3.93	-	-
	green	024A-F	245	1 to 14	10.07	-	-3.93	-	-
NaCl	green	23	245	14	10.07	-	-3.93	0.36	-
NaCl	green	27	254	14	10.07	-	-3.93	0.36	-

^a Green fluorite intergrown with minor purple fluorite; reacted solutions controlled by green fluorite composition.

Table 3: Major element compositions (logarithm molality) of the quenched experimental solutions and calculated pH (pH_T), solubility products ($Q_{\rm sp}$), and aqueous species activities at the experimental temperature. Ca and Na concentrations were measured using ICP-OES; F concentrations were measured using IC. The full dataset can be found in the Supplementary Materials.

Exp	Time	T	pH_T	$\log m \mathrm{Ca}$	$\log m \mathrm{Na}$	$\log m \mathbf{F}$	$\log m C$	$\log Q_{sp}$	$a\mathrm{HF}$	$a\mathrm{F}^-$	aCa ²⁺	aCaCl ⁺	$a \operatorname{CaCl}_2^0$	aCaF ⁺	a CaOH $^{-}$	aNaF ⁰
	(days	(°C)		(molkg)	(mol/kg) (mol/kg	(mol/k	g)								
Acidic	(pH 2)															
28	14	98	2.17	-2.81	-	-2.56	-1.97	-11.56	-2.58	-4.23	-3.10	-4.20	-9.37	-6.18	-11.14	-13.13
$40^{a,c}$	14	98	2.48	-2.52	0.36	-2.22	0.36	-11.22	-2.28	-3.63	-3.95	-2.92	-5.95	-6.44	-11.71	-3.37
003A	1	154	2.36	-2.57	-	-2.31	-1.98	-11.58	-2.31	-4.33	-2.92	-3.77	-8.13	-5.56	-9.50	-13.02
003B	4	154	2.34	-2.58	-	-2.30	-1.98	-11.61	-2.30	-4.34	-2.93	-3.78	-8.14	-5.58	-9.53	-13.03
003C	5	154	2.40	-2.53	-	-2.29	-1.98	-11.44	-2.30	-4.28	-2.89	-3.74	-8.10	-5.47	-9.43	-12.97
003D	6	154	2.40	-2.53	-	-2.28	-1.98	-11.41	-2.29	-4.27	-2.88	-3.73	-8.09	-5.46	-9.42	-12.96
003E	7	154	2.37	-2.56	-	-2.28	-1.98	-11.49	-2.28	-4.29	-2.91	-3.76	-8.12	-5.51	-9.48	-12.99
003F	14	154	2.38	-2.55	-	-2.29	-1.98	-11.50	-2.30	-4.30	-2.90	-3.75	-8.11	-5.51	-9.47	-12.99
5	14	154	2.40	-2.52	-	-2.22	-1.97	-11.30	-2.23	-4.21	-2.88	-3.72	-8.07	-5.40	-9.42	-12.91
$7^{a,c}$	14	154	2.62	-2.50	0.33	-2.20	0.34	-12.12	-2.23	-3.99	-4.14	-2.94	-5.24	-6.44	-10.49	-3.62
15^b	14	154	2.16	-3.04	-2.58	-2.81	-1.89	-13.46	-2.82	-5.04	-3.37	-4.13	-8.39	-6.73	-10.15	-7.31
34^a	14	204	2.59	-2.42	-	-2.12	-1.97	-11.74	-2.12	-4.44	-2.86	-3.36	-7.01	-5.04	-8.39	-12.89
$37^{a,c}$	14	204	3.33	-2.27	0.34	-1.97	0.34	-11.42	-2.03	-3.60	-4.21	-2.74	-4.42	-5.55	-9.03	-3.07
10^a	14	244	2.59	-2.43	-	-2.13	-1.97	-12.79	-2.13	-4.90	-2.98	-3.11	-6.19	-5.09	-7.99	-13.10
$12^{a,c}$	14	244	3.36	-2.32	0.36	-2.02	0.36	-12.72	-2.05	-4.06	-4.61	-2.84	-4.01	-5.87	-8.87	-3.36
20^{b}	14	245	2.52	-2.50	-2.58	-2.22	-1.89	-13.20	-2.22	-5.07	-3.06	-3.09	-6.06	-5.32	-8.12	-6.83
Mildly	acidic	(pH 4)														
42	14	98	4.36	-3.77	-	-3.47	-3.94	-11.01	-4.12	-3.59	-3.83	-6.85	-13.93	-6.27	-9.69	-12.44
29	14	98	4.82	-3.75	_	-3.51	-4.05	-10.94	-4.55	-3.56	-3.81	-6.93	-14.12	-6.22	-9.20	-12.41

-	_	
\subset	フ:	
0	. •	
•	~	۰

33	14	98	4.84	-3.82	-	-3.60	-4.05	-11.18	-4.66	-3.65	-3.87	-6.99	-14.18	-6.38	-9.25	-12.50
$31^{a,c}$	14	98	4.72	-3.45	0.34	-3.14	0.34	-12.25	-4.59	-3.69	-4.87	-3.85	-6.89	-7.41	-10.38	-3.44
001A	1	147	4.77	-3.85	-	-3.55	-4.05	-11.29	-4.16	-3.69	-3.91	-6.80	-13.26	-5.99	-8.21	-12.35
001B	4	147	4.79	-3.73	-	-3.41	-4.05	-10.90	-4.03	-3.55	-3.80	-6.70	-13.16	-5.74	-8.09	-12.21
001C	5	147	4.78	-3.75	-	-3.43	-4.05	-10.95	-4.04	-3.57	-3.82	-6.71	-13.17	-5.77	-8.11	-12.23
001D	6	147	4.89	-3.69	-	-3.38	-4.05	-10.76	-4.08	-3.50	-3.76	-6.66	-13.12	-5.64	-7.95	-12.16
001E	7	147	4.80	-3.71	-	-3.39	-4.05	-10.83	-4.02	-3.52	-3.78	-6.68	-13.14	-5.69	-8.05	-12.19
001F	14	147	4.86	-3.67	-	-3.36	-4.05	-10.71	-4.03	-3.48	-3.75	-6.64	-13.11	-5.61	-7.96	-12.14
19	6	154	5.13	-3.79	-	-3.54	-4.05	-11.12	-4.38	-3.63	-3.85	-6.70	-13.06	-5.80	-7.66	-12.26
$17^{a,c}$	14	154	5.08	-3.40	0.36	-3.10	0.36	-12.53	-4.44	-3.74	-5.05	-3.83	-6.11	-7.10	-8.95	-3.34
35	14	204	4.92	-3.80	-	-3.40	-3.94	-11.30	-3.72	-3.71	-3.89	-6.26	-11.78	-5.33	-7.08	-12.08
$38^{a,c}$	14	204	5.59	-3.06	0.38	-2.76	0.38	-12.09	-4.22	-3.53	-5.03	-3.52	-5.18	-6.30	-7.58	-2.97
21^b	14	245	3.34	-3.69	-1.97	-3.60	-1.93	-15.56	-3.64	-5.67	-4.22	-4.25	-7.23	-7.08	-8.46	-6.81
$22^{a,c}$	14	245	5.77	-3.03	0.38	-2.73	0.38	-12.62	-4.03	-3.64	-5.34	-3.55	-4.70	-6.17	-7.18	-2.92
25	14	254	5.73	-3.95	-	-3.70	-4.05	-11.93	-4.17	-3.93	-4.07	-6.04	-10.90	-5.06	-5.82	-11.95
26	14	254	5.36	-3.96	-	-3.54	-4.05	-11.93	-3.80	-3.93	-4.07	-6.04	-10.91	-5.05	-6.19	-11.94
Alkalin	е (рН	10)														
30	14	98	8.61	-3.83	-3.93	-3.70	-	-11.33	-8.50	-3.72	-3.89	-11.97	-	-6.46	-5.50	-7.49
$32^{a,c}$	14	98	8.02	-3.58	0.34	-3.28	0.34	-12.58	-7.98	-3.79	-5.00	-3.99	-7.04	-7.64	-7.22	-3.54
$41^{a,c}$	14	98	8.02	-3.41	0.34	-3.11	0.34	-12.08	-7.81	-3.62	-4.83	-3.81	-6.86	-7.31	-7.06	-3.37
6	14	154	7.64	-3.76	-3.93	-3.47	-	-10.84	-6.76	-3.49	-3.86	-11.66	-	-5.66	-5.15	-7.05
$18^{a,c}$	14	154	7.20	-3.24	0.36	-2.93	0.36	-12.00	-6.38	-3.56	-4.89	-3.66	-5.95	-6.75	-6.66	-3.16
36	14	204	6.63	-4.02	-3.93	-3.54	-	-11.26	-5.30	-3.57	-4.12	-11.54	-	-5.43	-5.60	-6.87
$39^{a,c}$	14	204	6.68	-3.03	0.37	-2.73	0.37	-11.95	-5.26	-3.48	-4.99	-3.50	-5.15	-6.21	-6.46	-2.93
043A	5	244	7.07	-3.97	-3.93	-3.63	-	-11.54	-5.38	-3.68	-4.19	-11.22	-	-5.07	-4.71	-6.71
043B	6	244	6.66	-4.16	-3.93	-3.64	-	-11.69	-4.99	-3.69	-4.31	-11.34	-	-5.20	-5.24	-6.72
043C	7	244	7.15	-3.94	-3.93	-3.65	-	-11.55	-5.48	-3.69	-4.17	-11.20	-	-5.06	-4.61	-6.72

043D	10	244	7.44	-3.79	-3.93	-3.73	-	-11.64	-5.85	-3.77	-4.10	-11.14	-	-5.08	-4.26	-6.80
11	14	244	6.53	-4.13	-3.93	-3.60	-	-11.59	-4.82	-3.66	-4.28	-11.31	-	-5.14	-5.34	-6.68
024A	1	245	7.20	-4.12	-3.93	-3.86	-	-12.14	-5.72	-3.89	-4.35	-11.37	-	-5.43	-4.72	-6.91
024B	4	245	7.09	-4.05	-3.93	-3.71	-	-11.76	-5.47	-3.75	-4.26	-11.28	-	-5.20	-4.75	-6.77
$024\mathrm{C}$	5	245	7.07	-4.10	-3.93	-3.74	-	-11.85	-5.47	-3.78	-4.30	-11.32	-	-5.26	-4.81	-6.80
024D	6	245	7.11	-3.97	-3.93	-3.65	-	-11.59	-5.43	-3.70	-4.19	-11.22	-	-5.08	-4.66	-6.72
024E	7	245	7.04	-4.09	-3.93	-3.72	-	-11.81	-5.42	-3.76	-4.29	-11.31	-	-5.24	-4.83	-6.78
024F	14	245	5.74	-4.32	-3.93	-3.53	-	-11.84	-4.07	-3.70	-4.43	-11.46	-	-5.33	-6.27	-6.72
$23^{a,c}$	14	245	6.48	-3.10	0.36	-2.79	0.36	-12.75	-4.79	-3.68	-5.39	-3.61	-4.77	-6.26	-6.52	-2.97
$27^{a,c}$	14	254	6.51	-2.96	0.36	-2.66	0.36	-12.52	-4.61	-3.59	-5.35	-3.50	-4.54	-5.99	-6.35	-2.83

^a Experiments with ~ 15 wt. % NaCl. ^b Experiments with 0.5 ppm REE doped. ^c Analytical difficulty with F on ion IC due to high sample chloride concentrations; F concentration calculated based on Ca concentrations ($mF=2\times mCa$).

Table 4: Rare earth element compositions (logarithm molality) of the quenched experimental solutions measured using solution ICP-MS.

Exp	Time	e T	$\log m \text{La}$	$\log m \mathrm{Ce}$	$\log m \Pr$	$\log m \mathrm{Nd}$	$\log m \mathrm{Sm}$	$\log m \mathrm{Eu}$	$\log m Gd$	$\log m \text{Tb}$	$\log m \mathrm{Dy}$	$\log m Y$	$\log m \mathrm{Ho}$	$\log m \mathrm{Er}$	$\log m \mathrm{Tm}$	$\log m Y b$	$\log m \mathrm{Lu}$
	(days	s)(°C)	(mol/kg) (mol/kg)	(mol/kg	(mol/kg)	(mol/kg)	(mol/kg	(mol/kg)	(mol/kg)	(mol/kg)	(mol/kg) (mol/kg)	(mol/kg)	(mol/kg)	(mol/kg)	(mol/kg)
Acid	ic (pl	H 2)															
28	14	98	-6.67	-8.17	-9.04	-8.32	-8.19	-	-8.28	-8.54	-8.07	-6.75	-8.73	-8.22	-9.10	-8.41	-9.23
40	14	98	-	-	-	-	-	-	-	-	-	-	-	-	-	-	-
003A	1	154	-6.51	-7.20	-8.15	-7.59	-8.38	-8.80	-8.39	-9.33	-8.51	-7.49	-9.33	-8.93	-9.85	-9.10	-10.05
003B	4	154	-6.64	-7.15	-8.03	-7.43	-8.15	-8.66	-8.08	-8.92	-8.12	-6.96	-8.83	-8.40	-9.34	-8.59	-9.55
003C	5	154	-6.62	-7.08	-7.97	-7.38	-8.12	-8.63	-8.05	-8.88	-8.05	-6.88	-8.74	-8.31	-9.22	-8.46	-9.39
003D	6	154	-6.70	-7.23	-8.12	-7.52	-8.21	-8.66	-8.18	-9.03	-8.25	-7.24	-9.05	-8.64	-9.60	-8.86	-9.85
003E	7	154	-6.65	-7.17	-8.08	-7.51	-8.22	-8.63	-8.18	-9.05	-8.26	-7.21	-9.03	-8.63	-9.55	-8.81	-9.74
003F	14	154	-6.62	-7.13	-8.00	-7.46	-8.18	-8.63	-8.14	-8.99	-8.18	-7.10	-8.95	-8.54	-9.46	-8.73	-9.66
5	14	154	-6.92	-7.31	-	-7.61	-	-7.66	-	-	-	-7.44	-	-	-	-	-
7	14	154	-6.70	-7.13	-8.02	-7.46	-	-	-7.99	-	-	-7.03	-8.90	-	-	-	-
15	14	154	-5.44	-5.48	-5.48	-5.48	-5.50	-5.50	-5.52	-5.52	-5.53	-5.26	-5.54	-5.54	-5.55	-5.56	-5.56
34	14	204	-7.02	-7.01	-8.76	-7.98	-7.72	-8.66	-	-8.24	-7.80	-6.55	-8.46	-8.00	-8.90	-8.18	-9.10
37	14	204	-6.67	-5.02	-	-	-5.93	-	-	-6.58	-	-	-	-7.03	-	-	-
10	14	244	-7.14	-7.30	-	-7.52	-	-	-7.99	-	-	-6.97	-	-	-	-	-
12	14	244	-6.71	-6.85	-	-7.11	-	-	-7.52	-	-8.45	-	-	-7.67	-	-8.30	-
20	14	245	-6.18	-6.19	-6.21	-6.24	-6.27	-6.28	-6.33	-6.28	-6.25	-6.12	-6.26	-6.23	-6.18	-6.11	-6.12
Mild	ly ac	idic (p	H 4)														
42	14	98	-8.35	-8.55	-9.48	-8.90	-8.39	-9.49	-9.55	-8.75	-8.88	-8.48	-10.30	-9.33	-	-	-
29	14	98	-8.44	-8.54	-	-	-8.40	-9.05	-9.62	-8.75	-9.62	-8.46	-10.30	-9.31	-	-	-10.52
33	14	98	-8.13	-8.46	-9.03	-8.74	-8.32	-8.89	-8.86	-8.55	-8.87	-8.37	-8.91	-8.85	-9.09	-9.17	-9.20
31	14	98	-6.67	-5.02	_	_	-5.94	_	-	-6.58	_	-7.10	_	-7.03	_	_	_

-	≺	1
2	5	5

001A	1	147	-8.56	-8.72	-9.89	-9.19	-	-	-10.00	-	-10.05	-8.97	-11.00	-	-	-	-
001B	4	147	-8.82	-8.94	-9.82	-9.19	-	-	-10.22	-	-	-9.24	-	-	-	-	-
001C	5	147	-8.72	-8.82	-9.66	-9.08	-	-	-9.89	-	-10.00	-9.00	-10.70	-10.52	-	-	-
001D	6	147	-9.17	-9.60	-10.52	-9.64	-	-	-9.96	-	-10.00	-8.97	-10.70	-10.52	-	-	-
001E	7	147	-8.72	-8.92	-9.80	-9.35	-	-	-10.30	-	-	-9.64	-	-	-	-	-
001F	14	147	-9.11	-9.19	-10.22	-9.54	-	-	-	-	-	-	-	-	-	-	-
19	6	154	-7.96	-8.06	-8.36	-8.32	-8.51	-8.60	-8.54	-8.72	-8.73	-8.12	-8.80	-8.81	-8.89	-8.86	-8.88
17	14	154	-	-5.06	-	-5.57	-6.00	-	-	-6.56	-7.23	-	-7.43	-	-7.39	-	-7.38
35	14	204	-8.49	-8.76	-9.74	-9.19	-8.39	-9.70	-9.72	-8.75	-9.80	-8.65	-10.70	-9.33	-	-10.22	-
38	14	204	-6.66	-4.96	-7.28	-	-5.78	-6.79	-	-6.33	-	-6.82	-	-6.71	-	-	-
21	14	245	-4.97	-5.28	-5.64	-5.61	-5.44	-5.57	-5.60	-5.46	-5.56	-5.30	-5.56	-5.40	-5.55	-5.55	-5.56
22	14	245	-	-5.05	-	-7.20	-5.97	-7.62	-6.81	-	-	-	-	-	-	-	-
25	14	254	-7.96	-8.03	-8.17	-8.19	-7.97	-8.14	-8.19	-8.07	-8.16	-7.97	-8.26	-8.22	-8.34	-8.35	-8.36
26	14	254	-8.57	-9.14	-9.82	-8.96	-8.40	-	-9.64	-8.75	-	-8.79	-10.40	-9.15	-10.52	-10.15	-10.40
Alka	line (pH 10	0)														
30	14	98	-9.55	-8.94	-	-9.80	-8.39	-9.77	-	-8.76	-	-8.82	-	-9.59	-	-	-
32	14	98	-6.72	-5.01	-	-	-5.88	-	-	-6.53	-	-	-	-6.99	-	-	-
41	14	98	-	-	-	-	-	-	-	-	-	-	-	-	-	-	-
6	14	154	-9.12	-	-10.00	-7.83	-	-7.85	-	-	-	-	-	-	-	-	-
18	14	154	-	-5.05	-	-7.08	-6.01	-7.46	-6.72	-6.60	-	-	-	-7.29	-	-	-
36	14	204	-9.77	-9.09	-	-	-8.37	-9.77	-	-8.77	-11.00	-	-	-9.49	-	-	-
39	14	204	-6.62	-4.76	-6.72	-	-5.02	-6.42	-6.43	-5.10	-	-6.54	-	-6.18	-	-	-7.50
043A	5	244	-9.34	-8.63	-10.22	-	-8.37	-9.70	-8.59	-8.75	-	-9.39		-9.42	-	-	-
043B	6	244	-9.59	-9.28	-9.64	-9.89	-8.38	-9.62	-	-8.76	-	-9.62		-9.39	-	-	-
043C	7	244	-8.95	-8.43	-8.62	-8.86	-8.27	-9.59	-9.64	-8.74	-9.85	-8.90	-10.15	-9.43	-10.22	-	-
043D	10	244	-8.70	-8.36	-8.39	-8.73	-8.31	-9.43	-9.26	-8.74	-	-8.56	-10.40	-9.10	-	-	-
11	14	244	-8.74	-9.30	-10.00	-9.49	-	-10.10	-9.62	-10.22	-	-9.27	-10.15	-	-10.22	-	-10.22

024A 1	245	-9.66	-9.11	-	-	-8.41	-	-	-8.78	-	-9.15	-10.70	-9.52	-	-	-10.52
024B 4	245	-9.42	-8.47	-10.15	-8.73	-8.35	-9.22	-	-8.79	-	-9.12	-10.30	-9.24	-10.15	-10.00	-10.05
024C 5	245	-9.52	-9.19	-9.89	-	-8.39	-9.23	-	-8.75	-	-9.15	-11.00	-9.21	-	-	-
024D 6	245	-9.37	-8.62	-9.96	-9.24	-8.34	-	-9.60	-8.75	-	-9.34	-10.70	-9.35	-	-	-
024E 7	245	-8.16	-8.10	-8.29	-8.32	-8.11	-8.38	-8.32	-8.42	-8.75	-8.23	-8.80	-8.67	-8.87	-8.90	-8.88
024F 14	245	-8.16	-8.16	-8.24	-8.24	-8.04	-8.32	-8.34	-8.25	-8.45	-8.20	-8.49	-8.40	-8.58	-8.63	-8.64
23 14	245	-	-5.05	-	-	-5.99	-	-6.79	-6.60	-	-	-	-	-	-	-
27 14	254	-6.55	-5.05	-	-	-6.01	-	-	-6.59	-	-	-	-	-	-	-

Table 5: Experimental solubility data ($\log Q_{sp}$) selected between 25–254 °C for deriving the fluorite solubility constants ($\log K_{sp}$, Eq. 1) as a function of temperature with regressed coefficients (A-D; with T in Kelvin) and derived standard Gibbs energy ($\Delta G^{\circ}_{298.15K}$), enthalpy ($\Delta H^{\circ}_{298.15K}$) and entropy $\Delta S^{\circ}_{298.15K}$ at 298.15 K and 1 bar. Subscripts indicate properties of formation from the elements ($_f$) and of reaction ($_r$).

	T (°C)	T (K)	$1000/T (K^{-1})$	$\log Q_{\mathrm{sp}}$	1σ	Refs
Experimental data	25	298	3.35	-10.62	0.02	[2]
	50	323	3.09	-10.45	0.03	[2]
	25	298	3.35	-10.51	0.01	[3]
	100	373	2.68	-10.41	0.04	[4]
	147	420	2.38	-10.77	0.09	[1]
	154	427	2.34	-10.98	0.19	[1]
	204	477	2.10	-11.28	0.03	[1]
	244	517	1.93	-11.59	0.05	[1]
	245	518	1.93	-11.82	0.02	[1]
	254	527	1.90	-11.93	0.01	[1]
Fit	25	298	3.35	-10.56		[1]
Equation		A	В	С	D	
$\log K_{\rm sp} = A + BT + C/T + D\log(T)$		171.180	0.01477	-7794.10	-64.6634	[1]
Thermodynamic properties		Values	Units			
$\Delta_r \mathrm{G}^{\circ}{}_{298.15K}$		60.29	$(kJmol^{-1})$			[1]
$\Delta_r \mathrm{H}^{\circ}{}_{298.15K}$		14.05	$(kJmol^{-1})$			[1]
$\Delta_r \mathrm{S}^{\circ}_{298.15K}$		-155.1	$(\mathrm{Jmol^{-1}K^{-1}})$			[1]
$\Delta_f \mathrm{G^{\circ}_{fluorite}}$		-1176.6	$(kJmol^{-1})$			[1]
		-1175.3	$(kJmol^{-1})$			[5]
$\Delta_f \mathrm{H^{\circ}_{fluorite}}$		-1227.9	$(kJmol^{-1})$			[1]
		-1228.0	$(kJmol^{-1})$			[5]
$S^{\circ}_{\text{fluorite}}$		72.3	$(\mathrm{Jmol}^{-1}\mathrm{K}^{-1})$			[1]
		68.9	$(\mathrm{Jmol}^{-1}\mathrm{K}^{-1})$			[5]
$\Delta_f \mathrm{G^{\circ}_{Ca^{2+}}}$		-552.82	$(kJmol^{-1})$			[6]
$\Delta_f \mathrm{H^{\circ}_{Ca^2+}}$		-543.10	$(kJmol^{-1})$			[6]
$S^{\circ}_{Ca^{2+}}$		-56.5	$(\mathrm{Jmol^{-1}K^{-1}})$			[7]
$\Delta_f \mathbf{G^{\circ}}_{\mathbf{F}^{-}}$		-281.75	$(kJmol^{-1})$			[7]
$\Delta_f \mathrm{H}^{\circ}{}_{\mathrm{F}^{-}}$		-335.39	$(kJmol^{-1})$			[7]
$S^{\circ}_{F^{-}}$		-13.2	$(\mathrm{Jmol}^{-1}\mathrm{K}^{-1})$			[7]

[1] This study; [2] Henry (2018); [3] Garand and Mucci (2004); [4] Richardson and Holland (1979); [5]

Robie and Hemingway (1995); [6] Sucprt92 (slop98.dat) optimized by Miron et al. (2017); [7] Sucprt92 (slop98.dat), Sverjensky et al. (1997) 68